CHAPTER 82

Magnetic Resonance Angiography: Physics and Instrumentation

Oliver Wieben and Thorsten Bley

Magnetic resonance imaging (MRI) provides several useful approaches for the assessment of vascular disease. Signal properties of flowing blood can be exploited to differentiate the blood pool from stationary tissue with positive (bright blood imaging) or negative (black blood imaging) contrast and to provide functional information in terms of velocity maps and flow measurements. In another technique, contrast-enhanced MR angiography (CE-MRA), a venously injected gadolinium (Gd) chelate contrast agent mixes with blood and alters its signal properties. The major advantage of MR angiography (MRA) is the capability to capture comprehensive information for all voxels within a larger three-dimensional imaging volume, allowing for the display of torturous vessel paths in various modes and for reformatting of data for viewing in arbitrary planes. MRA is noninvasive, with only a venous puncture in the case of CE-MRA, and provides information about the surrounding soft tissues. Other MRI sequences can be added to extend the scope of the examination (e.g., vessel wall imaging, diffusion and perfusion imaging, functional MRI studies).

The performance of an MRA requires attention to detail because overall scan time must be optimized to provide sufficiently high spatial resolution for diagnosis. Typically, the operator must balance concerns related to anatomic coverage with the constraints placed on proper spatial resolution and overall scan time or temporal resolution. Prolonged MRA scan times increase the acquisition's susceptibility to image blurring artifacts from bulk body motion and physiologic motion related to respiration and cardiac contraction.

There have been dramatic improvements in MR hardware and acquisition approaches over the past decades, many of which have proved beneficial for or were inspired by angiography applications; these now allow for more rapid imaging with improved image contrast and reproducible image quality. This chapter discusses some underlying physical principles of vascular imaging using MRI and the instrumentation and acquisition approaches for typical MRA examinations. In addition, the various mechanisms for vascular bright blood vascular depiction using CE-MRA, time-of-flight MRA (TOF MRA), phase contrast MRA, and steady-state free precession MRA will be discussed. It should be noted that the terminology for MR techniques can sometimes be confusing, not only because there are many variants of related schemes, but also because various vendors usually market these technologies under different trade names.[1]

DATA ACQUISITION AND IMAGE RECONSTRUCTION

MRI is based on the nuclear magnetic resonance phenomenon, which arises in atoms with an odd number of protons and/or an odd number of neutrons. Almost all clinical MRI, including angiography applications, is based on the signal from the hydrogen nucleus, ^{1}H, a single, positively charged proton that is the most abundant in the body (mainly in H_20 but also in fat and other compounds). From a classic physics perspective, each proton has a magnetic dipole moment and behaves like a tiny bar magnet when interacting with a magnetic field. In the absence of an external magnetic field, the axes of the magnetic dipole moments are randomly arranged so that they in aggregate cancel each other out and result in a net magnetization of zero. However, in the presence of an external magnetic field, or B_0, the magnetic dipole moments of the protons will align parallel or antiparallel with the external field. In thermal equilibrium, slightly more spins are aligned parallel than antiparallel with the

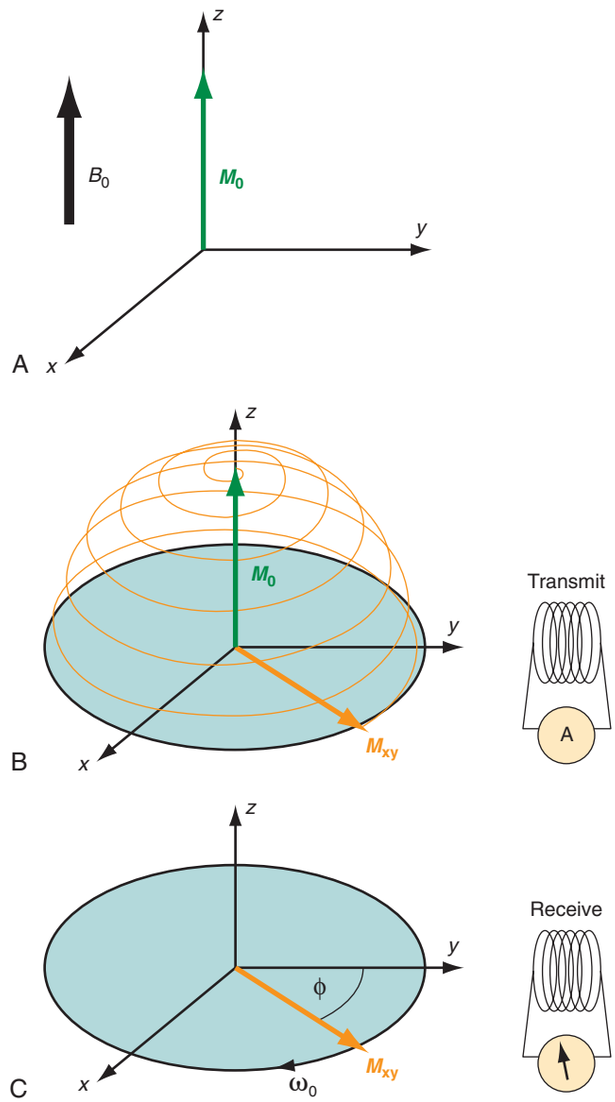

■ **FIGURE 82-1** **A,** In thermal equilibrium, the net magnetization is aligned with the direction of the main magnetic field, B_0. **B,** With an RF system that generates a RF field tuned to the resonance frequency of the spin ensemble, the net magnetization (M_0) can be tipped into the transverse plane. **C,** The transverse magnetization, M_{xy}, precesses at the Larmor frequency, ω_0, thereby creating an oscillating signal that can be measured with a receiver coil.

external magnetic field because it requires less energy. The result is a net magnetization that becomes the signal source in MR experiments. As shown in Figure 82-1A, this vector quantity is aligned with the direction of the main magnetic field. To measure signal from the net magnetization, it has to be "tipped" away from its orientation along the main magnetic field into the transverse plane. Once it is tipped away from the longitudinal axis, the magnetization vector rotates, or precesses, around that axis with a characteristic frequency, as given by the Larmor equation:

$$\omega_0 = -\gamma B_0 \qquad (1)$$

where ω_0 is referred to as the Larmor frequency, γ is the gyromagnetic ratio of protons (42.58 MHz/T) and B_0 is the magnetic field flux of the main field. The precessing transversal magnetization M_{xy} creates a weak radiofrequency (RF) field that can be recorded with a properly tuned coil (e.g., 63.87 MHz at B_0 = 1.5 T) circularly polarized about the axis of precession. As illustrated in Figure 82-1B, the tipping of the net magnetization vector is accomplished with a second RF system that can generate an oscillating magnetic field, B_1, close to the resonance frequency, a concept called RF excitation. In practice, the RF pulse is played out very shortly (in the order of milliseconds) and a remarkably small B_1 field is sufficient for RF excitation (e.g., ~50 mT in comparison to B_0 = 1.5 T).

Once the RF field is turned off, the spin system returns into its thermal equilibrium state. The rate of regrowth for the longitudinal magnetization follows an exponential waveform described by its characteristic time constant, called T1, referred to as the longitudinal relaxation time. The regrowth rate depends on the properties of the nucleus and its interactions with the environment. Meanwhile, the signal decrease in the transversal magnetization component is described by the exponential time constant called T2, the transversal relaxation time, and reflects dephasing caused by interactions between neighboring nuclei; also, it does not depend on the nucleus or chemical compound alone. Additional parameters contribute to the T2 relaxation, so that the T1 and T2 relaxation processes cannot be predicted from one another.

Multiple RF excitations are needed to acquire enough data for a two-dimensional image. The time between successive excitations is controlled by the MRI parameter repetition time (TR). The time between an RF excitation and the recording of the signal is controlled by the MRI parameter echo time (TE). Both of these parameters have an impact on the measured MR signal because they dictate how much time is allowed for the decay of the transversal magnetization (TE) or the regrowth of the longitudinal magnetization (TR). The actual measured MR signal depends on the T1 and T2 relaxation times, proton density, choice of TR and TE, and other imaging parameters, but also on factors such as motion, diffusion, and temperature. In MRA, the goal is to generate high signal differences between blood and surrounding background tissues, which is achieved by incorporating the motion of the blood using noncontrast MRA techniques or T1 shortening of blood by a circulating Gd chelate contrast agent using CE-MRA. Typical relaxation times are T1/T2 = 1200/250 ms for arterial blood and T1/T2 = 1200/220 ms for venous blood at 1.5 T.[2] Whereas T1 increases with field strength for most tissues (1600 ms for arterial blood), the T2 undergoes a small decrease.

Image Encoding

To create an image, the spatial distribution of the protons has to be resolved. Spatial encoding is achieved with the use of spatially and temporally varying magnetic fields. In the first step, the signal-generating volume is reduced to a slice (two-dimensional imaging) or volume (three-dimensional imaging) by selective excitation. A linear magnetic field gradient is superimposed onto the main magnetic field in the slice (or volume) direction simultaneously with the RF excitation. Consequently, the resonance frequency

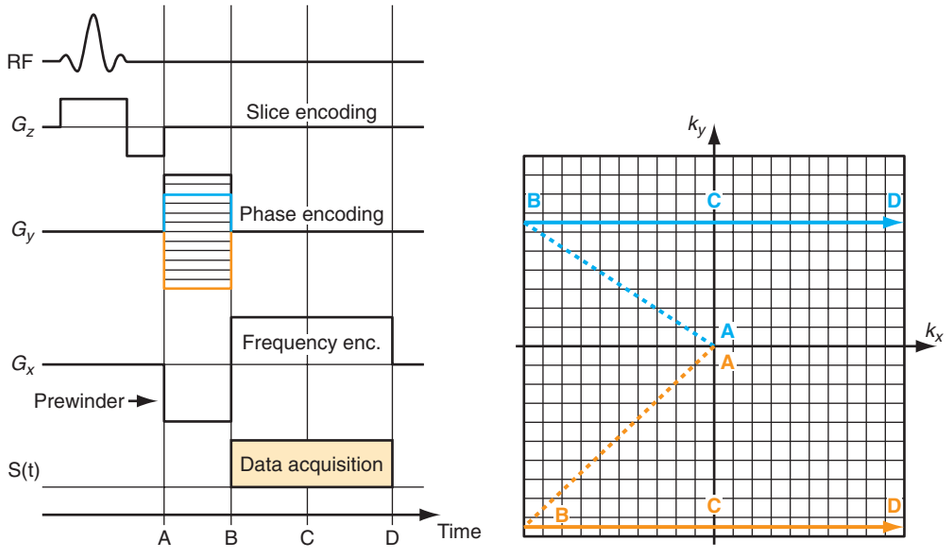

■ **FIGURE 82-2** Basic gradient echo pulse sequence for two-dimensional Fourier transform k-space scanning. An RF pulse and slice-encoding gradient, followed by a refocusing gradient, are played out simultaneously to excite spins in a slice. Frequency encoding is achieved with a linear gradient applied during data acquisition, resulting in the sampling of k-space along the frequency encoding direction k_x. A prewinding gradient is required to start the acquisition with negative spatial frequencies. The measurement is repeated with stepwise changing phase-encoding gradients for sampling along the frequency-encoding direction with different offsets in the phase- encoding direction k_y. The signed area under the gradients steers the sampling path, here shown for two phase-encoding settings (orange and blue) and their characteristic time points A, B, C, and D.

of the spin system is linearly varying as well. The RF system generates a pulse that excites not only a single precession frequency but all the frequencies contained in the desired slice or volume. Spins located outside the desired volume are not excited because their precession frequency is higher or lower than the frequency band covered by the RF excitation. Theoretically, this concept could be repeated in orthogonal directions ultimately to excite only a single point in the object, and then repeat the measurement until all points in the image are sampled. However, a much more efficient approach is Fourier encoding, whereby each sampled signal contains contributions from all spins in the object, therefore dramatically increasing the SNR of the acquisition. Figure 82-2 shows a basic example for a Fourier-encoded two-dimensional acquisition in the form of a pulse sequence diagram that illustrates the timing for RF excitation, the gradients, and data acquisition.

A second linear field gradient, called the frequency-encoding gradient, is applied during data sampling so that the precession frequency of the net magnetization varies linearly. Thus, the detected signal becomes a summation of all encoded frequencies and its spatial distribution can be derived by a one-dimensional Fourier transform. This encoding scheme makes MRI a spectroscopic imaging method. Unfortunately, the second spatial dimension cannot be encoded simultaneously during readout because this would result in a nonunique allocation of frequency and spatial location. Instead, the gradients are applied sequentially, with the drawback of extended imaging times.

The third gradient, called the phase-encoding gradient, is switched on and off prior to the frequency-encoding gradient. This leads to a linearly varying phase of the net magnetization vectors along the direction of that gradient, providing encoding for a single spatial frequency. In other words, with properly controlled gradients, the time-dependent MR signal actually samples the spatial frequencies of the object in two dimensions. Figure 82-2 shows how the sampling trajectory in the spatial frequency space, also called k-space, is controlled by the area under the gradient waveforms.

If that experiment is repeated several times with varying phase-encoding gradients, then multiple spatial frequencies are sampled in the phase-encoding direction as well and an image can be reconstructed via inverse two-dimensional Fourier transform. Figure 82-3 shows an example of a sagittal head scan. The received signal is digitized by an analog to digital converter and a discrete inverse two-dimensional Fourier transform generates the corresponding image, which contains magnitude (length of the transversal magnetization) and phase information (position in the transverse plain in respect to the coil axis) for each voxel. Most MRI relies on the magnitude image only. However, in some applications, such as phase contrast MRA, the phase information plays an essential role in generating image contrast.

Suppose an acquisition matrix contained 256 data points in the frequency and 256 data points in the phase-encoding direction. The reconstructed image is also described by a 256 × 256 matrix. For a two-dimensional acquisition, the total scan time is given by the number of phase- encoding steps multiplied by the repetition time (i.e., TR). Volumetric imaging can be accomplished by successive imaging of two-dimensional slices (i.e., two-dimensional MRA), or by excitation of an entire imaging volume (i.e., three-dimensional MRA) and the use of phase encoding in the third dimension for a true three-dimensional data acquisition. Either option prolongs the total scan time proportional to the number of slices (two-

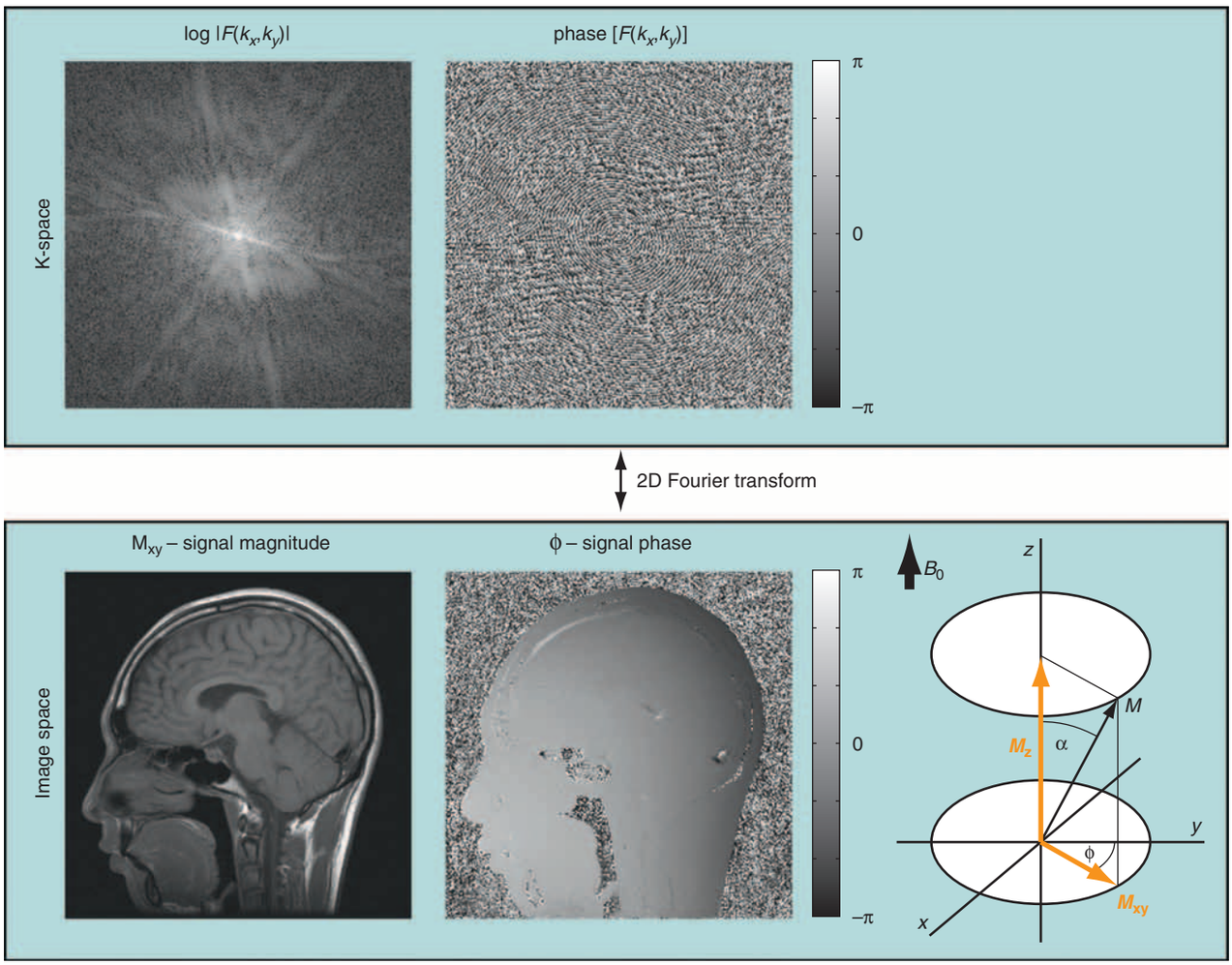

■ **FIGURE 82-3** Two-dimensional (2D) Fourier transform pair. The acquired complex k-space data are reconstructed into image space via a 2D Fourier transform. The resulting signal has a magnitude and a phase component, representing the transversal magnetization M_{xy} and its position ϕ in a unit circle in respect to a receiver axis. The highest signal can be obtained with a flip angle of $\alpha = 90$ degrees, which tips the magnetization vector completely into the transversal plane. Note that the k-space magnitude is shown on a logarithmic scale.

dimensional) or partitions (three-dimensional) in the volume.

Figure 82-4 provides some insight about the signal distribution in k-space. For this image, most of the signal energy is located around the origin of k-space. This area defines the weighting for the low spatial frequencies, which define the coarse outline of the imaged object yet lacks information on edges. The broad pattern of the phantom can be identified even with less than 0.5% of the k-space samples from the full-resolution image. However, all the detail is lost, which is defined in the unsampled higher spatial frequencies. The difference in images between the low-resolution images and the fully sampled image reveals the errors caused by limiting the acquisition to lower spatial frequencies only.

The basic signal-to-noise ratio (SNR) in MR acquisitions is given by

3

$$\text{SNR} \propto B_0 \times (\text{voxel volume}/\text{noise volume}) \times \sqrt{T_{acq}} \qquad (2)$$

where T_{acq} represents the data acquisition time.[3] Based on this relationship, one notes that the desirable properties for MRA, such as small voxel size for higher spatial resolution imaging and short acquisition times for fast scans, are detrimental to the obtainable SNR. Frequently, compromises in scan parameter choices are necessary for optimization of MRA for imaging individual vascular territories, with each offering unique challenges for proper visualization by MRA.

TECHNICAL REQUIREMENTS

The basic components of an MRI system are (1) a magnet that creates a strong static magnetic field, (2) an RF system that excites nuclei with a magnetic moment via RF pulses and detects the electrical signals created by the excited nuclei, and (3) a set of gradient coils that generates secondary static magnetic fields in a controlled fashion to

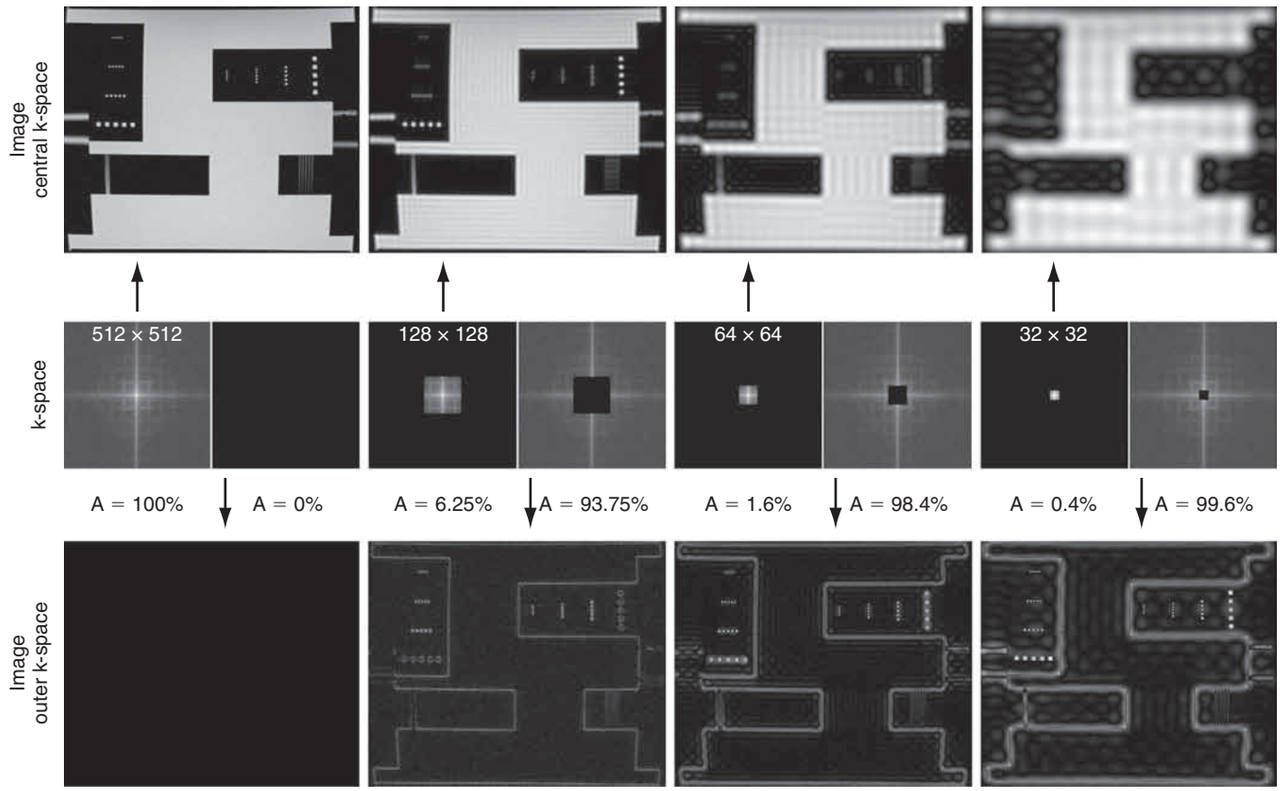

■ **FIGURE 82-4** A high-resolution phantom scan reconstructed from different k-space subregions. The upper row is reconstructed when the central 512 × 512 (full resolution), 128 × 128, 64 × 64, and 32 × 32 samples are used for the reconstruction. This is equivalent to using 100%, 6.25%, 1.6%, or 0.4% of all sampled data. The lower row represents reconstruction results when the remaining peripheral k-space data are used for the image reconstruction instead. Whereas the central k-space samples define the low spatial frequencies and most of the image contrast, the peripheral k-space data define the higher spatial frequencies and, therefore, fine structures and edges.

superimpose linear field gradients onto the main field for spatial encoding.

Magnetic Resonance Scanner

Each MR scanner is designed to provide a magnetic field, B_0, that is homogeneous over the imaging volume, stable over time, and against the influence of external sources. The magnetic induction of the field, also frequently referred to as the magnetic field strength is measured in tesla (T) or gauss (G), where 1 T = 10^4 G. The most common modern MR scanners used in clinical practice are whole-body scanners that rely on a superconducting magnet with a field strength of 1.5 or 3 T. For comparison, the field strength of a 1.5-T MR scanner is about 30,000 times stronger than the earth's magnetic field (~0.5 G). Superconducting MR scanners contain several coils that run in series to form a solenoid and create a cylindrically symmetrical magnetic field, with the main magnetic field aligned with the *z*-axis of the cylindrical housing (Fig. 82-5). They operate near absolute zero temperature (~4 K, or −270° C) effectively to eliminate electrical resistance in the coil wires, allowing large currents that generate high magnetic fields. Other MR scanner designs include resistive magnetic fields (without superconductivity) that operate at lower magnetic field strengths (<0.15 T), permanent magnetic fields that have intermediate field

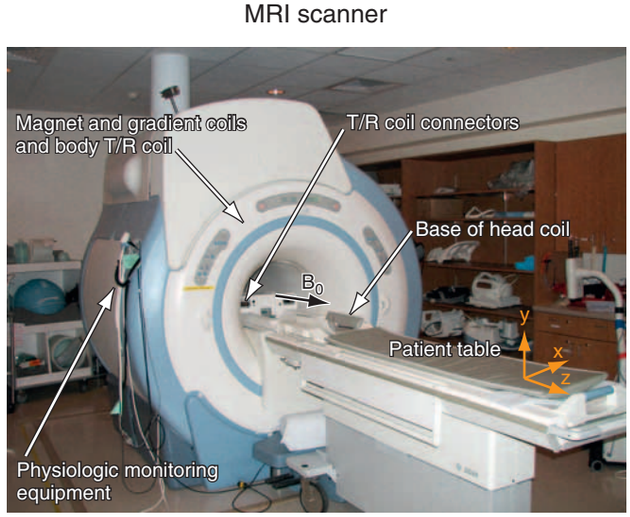

■ **FIGURE 82-5** A 1.5-T MR system with a superconducting magnet, gradient coils, and a body transmit-receive RF system enclosed in the housing. The patient table, connectors for external transmit-receive or receive-only coils, and physiologic monitoring equipment are also shown. The main magnetic field is aligned with the table axis, called the z-axis by convention.

■ **FIGURE 82-6** RF coils used for MR scanning. Bird cage coils for head **(A)** and knee **(B)** imaging are single-coil transmit and receive coils with a very homogeneous B_1 field. Single-channel surface coils such as the shoulder coil **(C)** or general purpose flex coil **(D)** are designed to have a high local sensitivity. Multielement coil arrays can combine the benefits of local sensitivity and larger coverage, here shown for an eight-channel neurovascular coil **(E),** eight-channel body phased- array coil **(F),** four-channel lower extremity coil **(G),** and eight-channel lower leg coil **(H).**

strength (<0.7 T), smaller bore diameter MR scanners for extremity imaging, and open bore designs (usually <0.7 T) to improve patient comfort and reduce claustrophobia. Imaging at lower field strengths reduces some of the problems encountered at higher fields, such as reduced RF penetration and increased energy absorption. However, MRA applications greatly benefit from imaging at higher field strength because the SNR increases linearly with field strength. MR scanners with field strengths of 3 T are becoming more prevalent in clinical settings and favorable results have been reported with these systems[4]; more recently, higher field 7-T research MR systems are being investigated.[5]

Gradient System

The magnetic field gradient system typically consists of three orthogonal gradient coils embedded within the housing of the scanner. Gradient coils are designed to produce a spatially varying magnetic field that can be temporally altered. Although these additional magnetic fields are dramatically smaller than the main magnetic field, they are an essential component for spatial encoding of the signal distribution in the imaging volume of interest. Gradients are rated by their maximum gradient strength (the higher the better) and the time needed to rise to the maximum gradient strength (slew rate—the faster the better). The gradient waveforms in Figure 82-2 are idealized in that they can be switched on and off instantaneously.

Gradient systems have undergone dramatic improvements over the last decade and modern equipment can provide maximum gradient strengths of about 50 mT/m and slew rates of 200 T/m/s. MRA applications greatly benefit from high-performance gradients because they enable faster imaging for higher temporal sampling of data, which can be used to improve spatial or temporal resolution. Faster imaging speeds are particularly helpful to assess the dynamic progression of a contrast bolus using multiphase or time-resolved MRA, or to ensure sufficient spatial resolution during a single breath-hold MRA acquisition. The minimization of imaging parameters such as the echo time, TE, or the repetition time, TR, are facilitated by the availability of high-performance gradients and provide additional benefits for image quality (see later).

Radiofrequency System

The RF system serves the purpose of converting pulsed oscillating currents from a power amplifier into an oscillating magnetic field, also referred to as the B_1 field, for the excitation of the nuclear spin system. This is accomplished by a transmitter coil tuned to the resonance frequency of the spin system under investigation. Such coils are designed to provide a uniform B_1 field over the imaging volume to ensure uniform spin excitation. So-called birdcage coils are well suited for this purpose and exist as whole-body coils built into the scanner housing and as specialty coils, such as for head or knee imaging (Fig. 82-6).

A receiver coil is used to detect the RF field created by the precessing magnetization of the nuclear spins after their excitation. The same coil may be used for transmitting and receiving the RF signals, which are referred to as transmit-receive coils (see Fig. 82-6A and B). However, in many applications, it is advantageous to use special local coils that are only sensitive to the signal from the region close to the coil. Such local coils can have a significantly better SNR, as described by equation 2, especially compared with the whole-body transmit-receive coil that encounters noise contributions from the whole volume within it that is much larger than that of smaller local coils. Figure 82-6 shows examples of such local coils, including a shoulder coil (C) and a multipurpose flex coil (D).

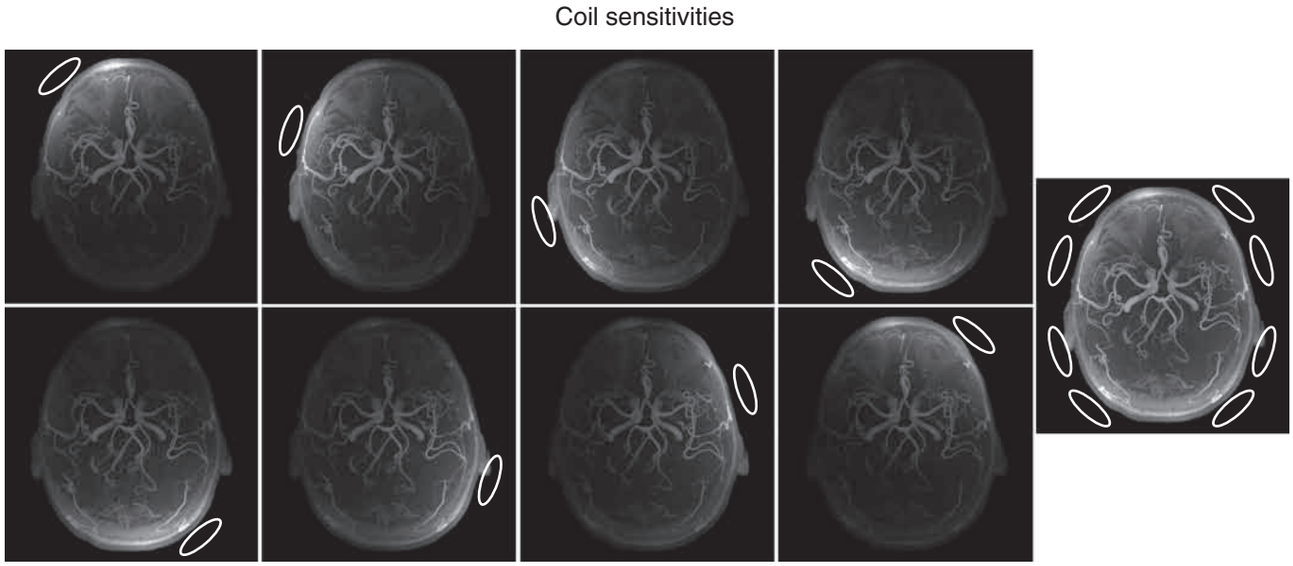

■ **FIGURE 82-7** TOF angiography data set acquired with an eight-channel head coil. Shown are images reconstructed for each individual coil with increased local sensitivity (small images) and after combining all images as the square root of the sum of the squares from all individual coil images. *(Courtesy of Dr. Alexej Samsonov, University of Wisconsin-Madison, Madison, Wis.)*

Coil arrays consist of multiple local receiver coils to provide a larger coverage with the SNR advantage of local coils. These multielement RF coils have become very common and are available for many applications in many body regions (Fig. 82-6E-H). Figure 82-7 demonstrates the local coil sensitivities of an eight-channel head coil in a two-dimensional TOF MRA and the cumulative image obtained from combining all channels. Data from multiple coils cannot be combined during acquisition and have to be stored individually. Therefore, the acquired data size increases linearly with the number of coils, and image reconstruction has to be completed for each channel before they can be combined. However, current reconstruction engines are prepared to handle the additional workload for 8 to 16 channels without significant delays.

Parallel Imaging

More recently, scan time reduction methods were developed that explore the redundancy in the information contained in multiple receiver coils with partly overlapping sensitivity regions. SMASH (***sim***ultaneous ***a***cquisition of ***s***patial ***h***armonics),[6] SENSE (***sens***itivity ***e***ncoding),[7] and GRAPPA[8] are acquisition and reconstruction methods from this group referred to as parallel imaging, which have found rapid commercial adaptation for cardiovascular imaging, especially CE-MRA. With this approach, the equivalent of multiple-phase encoding steps is acquired during a single readout. Although the advantage of accelerated imaging comes at the expense of a reduction in SNR, it can be highly beneficial in situations in which there is sufficient SNR and rapid image acquisition is desired. Basically, all CE-MRA applications fall into this category because faster imaging can improve the frame rate for dynamic acquisitions or reduce breath-hold lengths or other artifacts related to patient motion. As shown in Figure 82-8, attention has to be paid to potential local noise amplifications from the reconstruction process, frequently described as g-factor maps, when using high acceleration factors.

The scan time reduction factor that can be obtained with parallel imaging depends on the number of independent coil elements and their arrangement. Therefore, further increases in the number of coil elements and receiver channels promise even greater reductions in scan time. Consequently, the recent progress in parallel imaging has led to renewed interest in coil design and receiver systems. New MRI platforms provide the ability to connect many coil elements and acquire the signal from as many as 16 to 32 receivers simultaneously and systems with even more channels are being explored. With higher receiver coil counts, the SNR and coverage can be further improved or higher acceleration factors can possibly be obtained. Current design problems, such as with the decoupling of individual coil elements, has limited commercial coil designs to 8 to 32 elements. In research settings, systems with up to 128 receiver channels have been recently evaluated and demonstrated regional SNR benefits and high acceleration factors for cardiovascular applications as compared with lower count coil arrays.[9] However, the lack of penetration for small coils might limit additional benefits for regions of interest that are more distant from the body surface. It remains to be seen at which point additional coil elements are still beneficial, especially when the noise in the MR system becomes dominated by electrical noise from the receiver system, instead of intrinsic noise contributions caused by random motion of electrons in the patient's tissue.

Patient Monitoring

Patient monitoring systems are crucial components for vascular imaging because several approaches require synchronization with the cardiac cycle or feedback on the

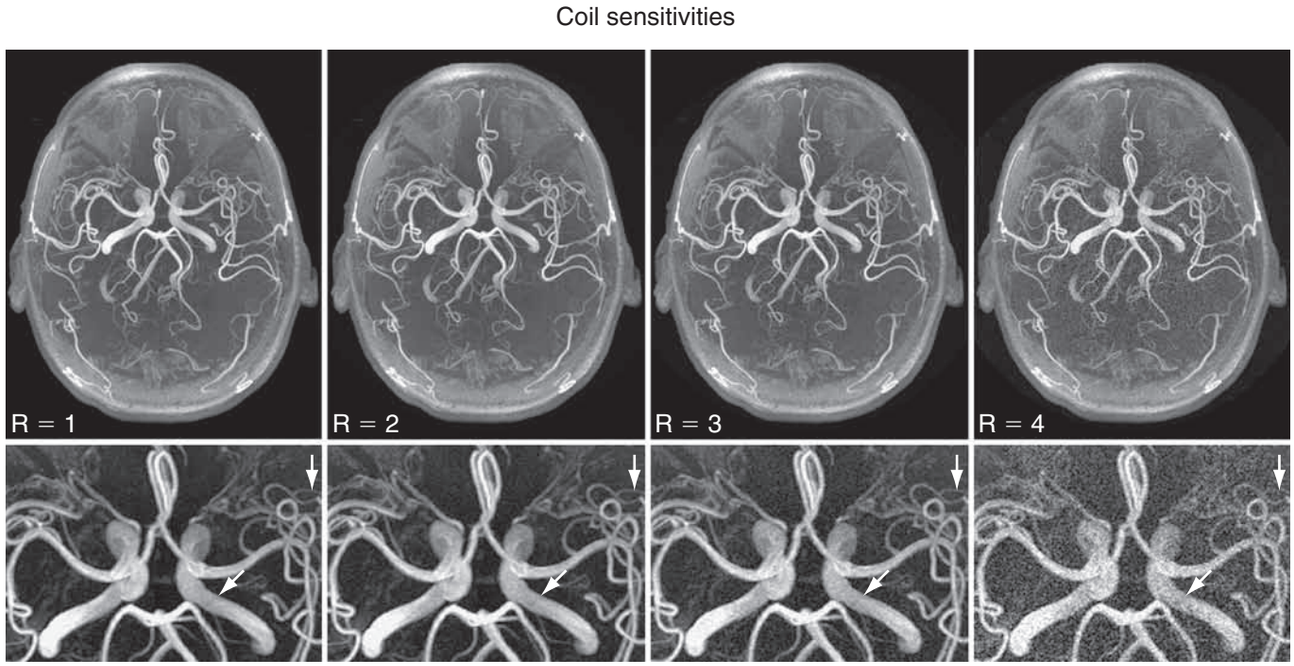

■ **FIGURE 82-8** MRA data reconstructed with a SENSE (1) based parallel imaging reconstruction using all the data from a fully sampled acquisition. The enlargements (*bottom row*) demonstrate good image quality for R = 2 but a decreased SNR and local noise enhancements for R = 3, which renders the images nondiagnostic, for a reduction of R = 4 with dramatic noise enhancements (*thick arrow*) that obscure vessel anatomy (*thin arrow*). 100% reduction factor R = 1; 50% (R = 2); 33% (R = 3); 25% (R = 4). *(Courtesy of Dr. Alexej Samsonov, University of Wisconsin-Madison, Madison, Wis.)*

18

respiratory motion for optimized image quality. To accommodate these needs, most MR systems are equipped with a pulse oximeter probe, an electrocardiogram (ECG) gating system, and stress transducer systems worn as a belt around the abdomen to track abdominal distention during respiration.

The most precise synchronization with the cardiac cycle is obtained with R wave detection from an ECG signal. It requires the placement of three or four MR-compatible electrodes on the subject's chest and the connection to an amplifier system. ECG readings from within the MR scanner are often suboptimal for proper diagnostic ECG interpretation because of magnetohydrodynamic effects, which most notably manifest themselves as enlarged T waves. These enlarged T waves can cause problems in gated acquisitions when they are mistaken as the trigger point from the R wave. Vector gating systems that process multiple leads simultaneously, as well as careful electrode placement, can minimize erroneous ECG gating results. Another source for suboptimal gating results can be unwanted signal perturbations into the ECG leads from gradient switching and RF transmission. Heavy shielding or shortening of the ECG cables can minimize these effects. Use of fiberoptic ECG cables for extended connections can also reduce these concerns. An alternative to ECG gating is to use optically based arterial blood oxygen saturation monitors (SaO_2) in the form of finger probes or reflectance probes for cardiac imaging synchronization. The setup for these measurements is simple but the signal has a less distinct peak within the cardiac cycle for gating, making it less desirable for acquisitions that need precise synchronization.

Stress transducer systems provide a similarly simple approach for the tracking of the respiratory cycle. However, they can lack precision because they track the abdominal circumference instead of the targeted image area, can undergo baseline drifts, and can pose difficulties in shallow breathers. A more precise but also more complex approach is the use of navigator echoes that track the position of the lung-liver interface (i.e., hemidiaphragm) and determine the respiratory cycle of the patient, typically during tidal respiration.

Power Injector

For CE-MRA, a Gd-based contrast agent is injected intravenously, usually into an antecubital vein. The injection of the contrast agent is followed by the injection of sterile saline to flush the contrast material out of the delivery system and ensure that the contrast bolus is sufficiently central within the body. Although manual injections are possible, the use of a computer-controlled, MR-compatible power injector is usually preferred. The power injector is more precise in delivering reproducible injection rates and its use omits the need for an operator in the scan room during imaging. Power injectors also provide features to assist in dynamic timed studies and breath-hold maneuvers and allow for multiphase injections. A typical system consists of a delivery component in the scan room and a user console in the operator room (Fig. 82-9). Manual injections have the advantage that the physician is right next to the patient and can better monitor the administration of contrast agent and the status of the patient.

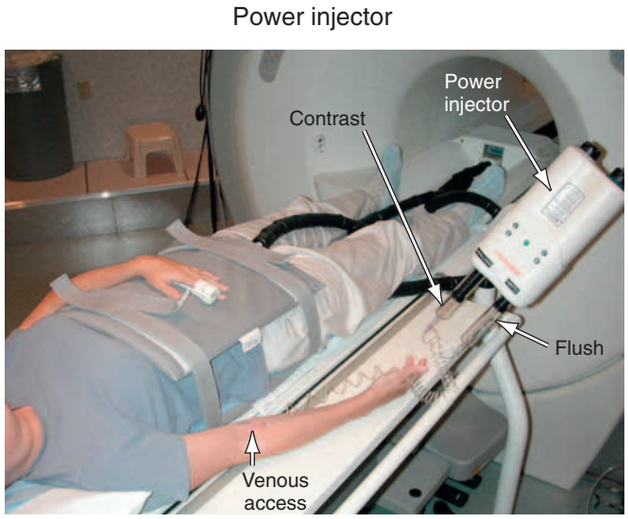

■ **FIGURE 82-9** MR-compatible power injector during patient preparation. A computer-controlled delivery system injects the contrast agent and the saline flush into the antecubital vein through a common line.

TECHNIQUES

Contrast-Enhanced Magnetic Resonance Angiography

CE-MRA[10] has quickly gained widespread clinical acceptance because of its ability to provide diagnostic angiographic data sets very quickly and reliably. In many practices, CE-MRA has replaced conventional x-ray angiography as the preferred method for angiographic depiction of specific anatomic regions such as the aorta, carotid arteries, and peripheral arteries.

The exposure to gadolinium-based contrast material has been associated with the development of nephrogenic systemic fibrosis (NSF).[11] Patients with compromised kidney function are at risk and proper screening (knowledge of the patient's renal function—estimated glomerular filtration rate [GFR] and serum creatinine level) is important to minimize potential risks. A more detailed discussion of NSF can be found in Chapter 18.

CE-MRA typically uses traditional extracellular MR contrast agents based on Gd, which is a paramagnetic metal ion that decreases T1 and T2 relaxation times. Because of the toxicity of Gd in pure form, it is chelated with ligands in formulations used in clinical practice. Basically, all CE-MRA acquisitions take advantage of the T1-shortening effect of the blood signal when it mixes with the Gd chelate contrast agent, resulting in a more rapid regrowth of the longitudinal magnetization. The MR acquisition is typically performed with a T1-weighted three-dimensional spoiled gradient echo pulse sequence with short TRs to maximize the contrast between the blood pool (high signal) and stationary tissue (low signal). The contrast medium bolus is intravenously administered, usually with a power injector at a fixed rate (e.g., 2 mL/sec) for single-station MRA examinations or possibly as a biphasic injection (e.g., 1.5 and 0.5 mL/sec). Both weight-based dosing (e.g., 0.2 mmol/kg Gd chelate contrast agent) and fixed dosing (e.g., 20 mL) of contrast medium can be used for CE-MRA, with the overall intent of reducing the T1 of blood to as low as 50 ms during the first pass. The specifics of the injection protocol should be tailored for the vascular territory, imaging pulse sequence, contrast agent, and specific condition and circulatory time of the patient. A discussion of specific MRA protocol considerations can be found elsewhere in this text in chapters that relate to the vascular territory and/or the underlying suspected pathologic condition (see Chapters ••).

The MR signal in CE-MRA is dominated by the T1-shortening effect of the blood signal caused by the presence of the circulating contrast agent and less by signal properties related to flowing blood. CE-MRA, in essence, provides a lumenogram similar to that of conventional x-ray angiography or CTA. T1 weighting is achieved with spoiled gradient echo pulse sequences with small flip angles and short TE and TR values. Short repetition times leave little time for signal regrowth between successive excitations and form the basis for good background suppression. Therefore, only tissues with a short T1 time will generate significant signal contributions (Fig. 82-10). A pitfall of this technique is its application in regions of the body where there is an abundance of fat in the surrounding background tissue. In these cases, the signal of surrounding fat may diminish the apparent contrast-to-noise discrimination of the arterial segments from signal of surrounding fat. Fat suppression or image subtraction of precontrast mask data sets can be used to improve the depiction of arteries on CE-MRA in such cases.

Bolus Timing for Contrast-Enhanced Magnetic Resonance Angiography

To optimize image quality, the data acquisition has to be synchronized with the contrast bolus transit through the target vasculature, which is typically arterial. The imaging objective is thus to capture critical image data during the arterial first passage of the bolus prior to contrast bolus progression and signal enhancement of the veins, and prior to significant dilution of the contrast bolus within the arterial tree (Fig. 82-11). Several approaches have been proposed to acquire the data during peak arterial Gd concentration so that a high SNR image without venous contamination is obtained. The simplest way to estimate the arrival time of the bolus is the best guess technique. However, this is also a highly inaccurate technique because the arrival time depends on a variety of parameters, such as the patient's cardiac output, size, and underlying vascular pathology.

Contrast bolus arrival time can be determined for an individual patient by performing a preliminary timing scan with a low dose of contrast agent (e.g., a 1- to 2-mL Gd chelate contrast agent test bolus).[12] With this method, a series of two-dimensional images of the target arterial tree is rapidly acquired (typically about one image/sec) and analyzed for arrival time of the test bolus into the artery under investigation. Based on these images, the arrival time for a full injection is predicted and a suitable delay time for the start of the data acquisition is determined. Disadvantages of the technique include a prolonged examination time for two injections and the use of additional

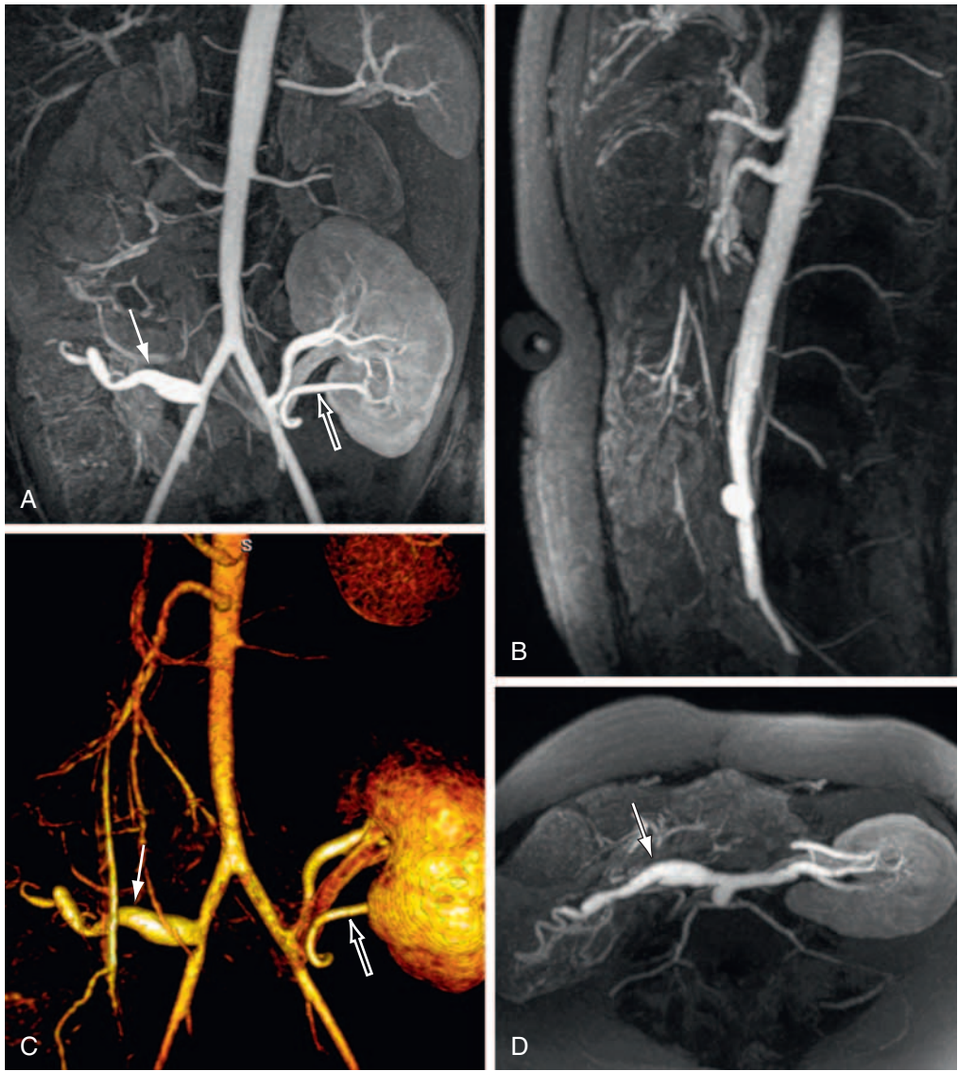

■ **FIGURE 82-10** Three-dimensional CE-MRA images from a patient who had undergone combined renal and pancreas transplantations displayed as coronal **(A)**, sagittal **(B)**, transversal **(D)** maximum intensity projection (MIP) images, with a volume-rendering technique (VRT) **(C)**. Note the patent pancreas transplant artery (*arrows*), renal transplant artery, and accessory renal transplant artery (*open arrows*).

19

contrast agent, which will necessarily increase the signal contributions of adjacent background tissues and the urinary system. Also, the arrival time of the contrast may vary because of differences in breathing or the initiation of a breath-hold.

Another timing method is to integrate an automated detection scheme that can monitor the signal in an arterial voxel[13] or a near–real-time two-dimensional image display (MR fluoroscopy) of the region of interest[14] that can be used to monitor for contrast bolus arrival and initiate the scan on arrival of the contrast bolus. These latter techniques have the advantage of a single injection for the CE-MRA itself and thus improved background signal suppression.

Magnetic Resonance Angiography Scan Time

Another consideration for CE-MRA is overall scan time for image acquisition. As noted, the duration of preferential arterial enhancement by the contrast bolus provides the ideal imaging window for CE-MRA. In some cases, such as with the carotid arteries, this window can be as brief as 5 seconds. Moreover, CE-MRA in the body is often improved if performed during a breath-hold because respiratory motion can result in significant blurring on CE-MRA. These time constraints limit the maximal achievable spatial resolution for a given three-dimensional MRA acquisition. For example, if one would want to acquire a cubic volume with an isotropic spatial resolution of 256 voxels in each dimension (Fig. 82-12A) and a typical TR of 5 ms, then the total scan time would be $T_{scan} = TR \times N_y \times N_{sl} = 328$ sec, where N_y and N_z represent the number of phase encoding steps in y and z. Instead, a reduced data set is sampled to limit the scan duration to 10 to 30 seconds, either with compromised spatial resolution by symmetrical k-space reduction (see Fig. 82-12B), reduced coverage (see Fig. 82-12C), asymmetrical reductions in k-space that maintain the spatial resolution by exploring

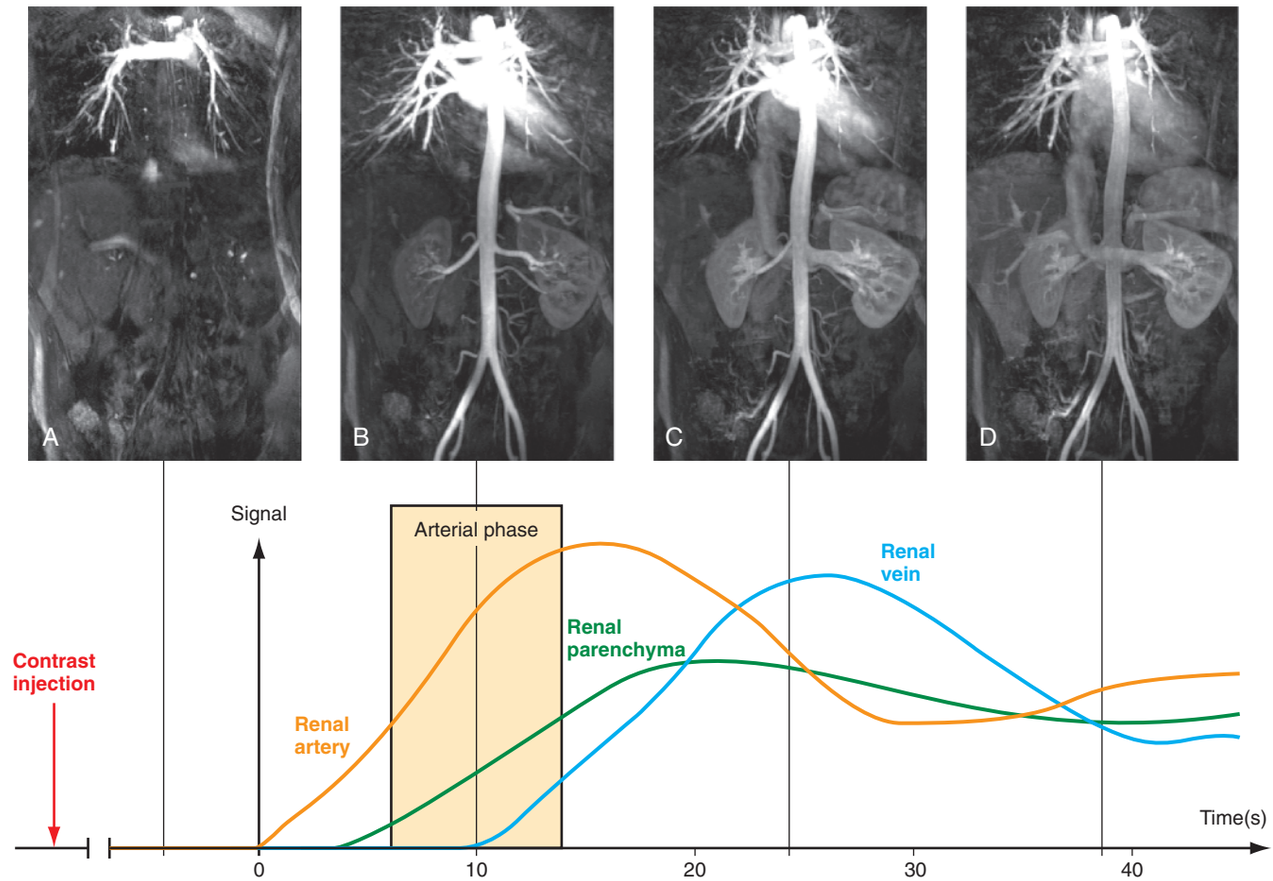

■ **FIGURE 82-11** Bolus passage in CE MRA with an extracellular contrast agent. After venous injection of the contrast agent, the bolus travels through the right ventricle, pulmonary system **(A)**, and left ventricle before it enters the systemic vasculature **(B)**. It then enters the venous system through the capillary bed **(C)** and transition of the contrast material from the intravascular compartment into interstitial space occurs **(C, D)**. Usually, images from the arterial phase **(B)** are desired to visualize arteries with high contrast to the surrounding tissue and veins.

symmetries in k-space (see Fig. 82-12D),[15] reduction of phase encoding steps with parallel imaging (see Fig. 82-12E),[6-8] or a combination of these techniques in a single- or double-phase encoding direction.

11

K-Space View Ordering

If it were possible to extend the scan time beyond the period of preferential arterial enhancement (i.e., arterial phase) without signal from the veins, the obtainable spatial resolution could be improved. To this end, sampling schemes have been developed that tailored the temporal order of the phase-encoding steps to optimize image quality. Because the central spatial frequencies (i.e., central k-space data) define the image contrast, it is necessary to acquire these portions of k-space during the peak of the arterial signal intensity, before the bolus arrives in the veins.[16] Higher spatial frequencies that dominate the edge information of an image (i.e., peripheral k-space data) can be acquired even after venous contamination to provide the desired spatial resolution with minimal signal interference from venous structures.

In traditional three-dimensional MR acquisition schemes, sequential phase-encoding schemes are applied (Fig. 82-13A). The first acquired view in such a scheme is the most distant from the origin of k-space. Line after line of k-space is acquired linearly by advancing one phase encode (here, k_z) from its minimum to its maximum while the other phase encode is kept constant (here, k_y). However, this scheme is not well suited to ensure sampling of the central k-space region during peak arterial enhancement. To this end, centric view-encoding k-space schemes were developed whereby the views near the k-space origin are acquired during the initial period of the scan. Centric view encoding k-space schemes facilitate better synchronization of key central k-space image data acquisition with the arrival of the contrast bolus. One such implementation is linear centric view encoding (see Fig. 82-13B), in which the views are ordered in a double loop; the outer one (here, k_y) is ordered based on its distance from the origin ($+\Delta k_y, -\Delta k_y, +2\Delta k_y, -2\Delta k_y, \ldots$) whereas the inner loop (here, k_z) is still chosen sequentially. A further optimized variation of this scheme is the so-called elliptical centric view ordering.[17] In this approach the temporal order of the acquisition of k-space lines is determined by their distance in the k_y-k_z plane to the center of k-space, providing a more compact and true centric encoding in both phase-encoding dimensions. The larger the distance between a k-space point and the origin, the later that particular k_x line is sampled (see Fig. 82-13C). When

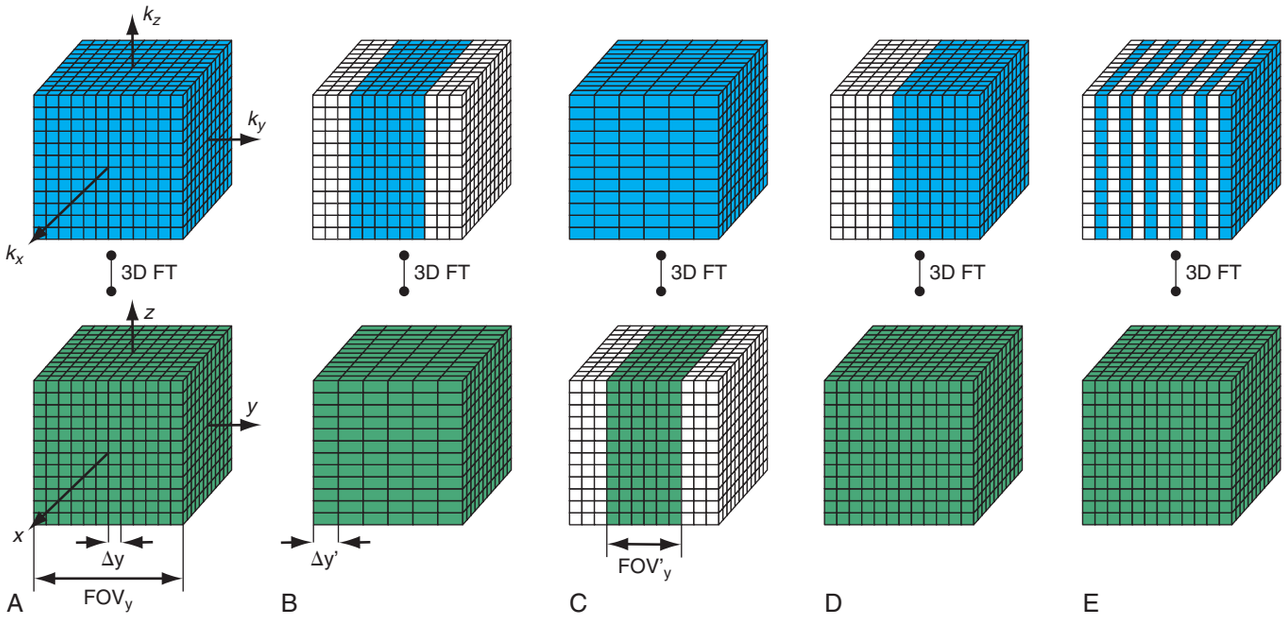

■ **FIGURE 82-12** With three-dimensional MR acquisitions, a volume in k-space is sampled and image volumes are reconstructed via three-dimensional Fourier transforms. High-resolution, large-coverage scans are time-consuming **(A)**. Scan time savings can be achieved a smaller matrix is sampled, such as with compromised spatial resolution in a phase-encoding direction **(B)**, reduced coverage in a phase-encoding direction **(C)**, partial Fourier acquisitions that assume certain symmetries in k-space **(D)**, reduction of phase-encoding steps with parallel imaging **(E)**, or a combination of these techniques. Here these schemes are shown for reductions in k_y but, in practice, they can also be used in k_z or in both phase encoding directions.

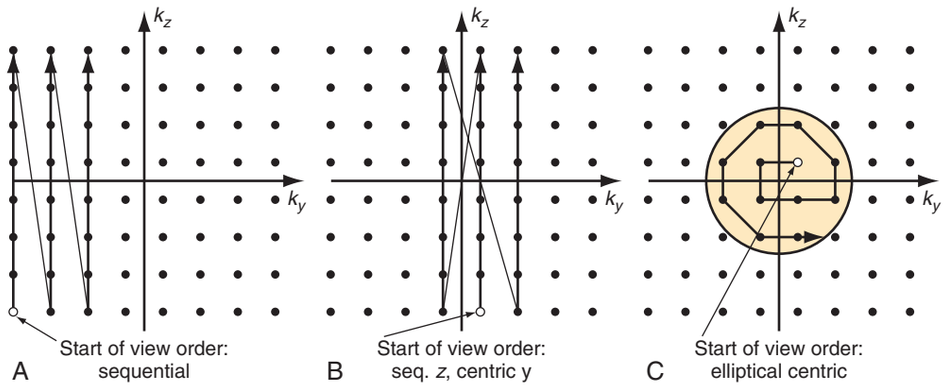

■ **FIGURE 82-13** View-ordering schemes for three-dimensional MRI . Each readout is represented by a dot and the readout direction is perpendicular to the shown k_y-k_z plane. **A,** Sequential phase encoding is well suited to image static objects. In CE-MRA, the limited time available to acquire data from arterial structures only is devoted to the contrast defining central k-space region, either with centric **(B)** or elliptical centric **(C)** view ordering. Only the first encoding steps are displayed in this figure.

properly timed, such ordering allows for the acquisition of the central k-space data during the signal intensity peak in the arteries and the higher spatial frequencies thereafter. It is also more robust to artifacts generated by the modulation of the contrast concentration and suppression of motion artifacts.[18] An example of such an acquisition is shown in Figure 82-10, demonstrating the large coverage, high spatial resolution, and three-dimensional reformatting capabilities of a CE-MRA data set acquired in a single breath-hold. Elliptical centric view ordering is particularly helpful for imaging arterial territories such as the carotid arteries, which can have especially brief periods of preferential arterial enhancement.

Time-Resolved Contrast-Enhanced Magnetic Resonance Angiography

Time-resolved CE-MRA has several advantages over the acquisition of a single time frame. With proper frame rates, arterial-only images are obtained without the need for any synchronization of the acquisition and arrival of the bolus. In addition, this technique provides temporal information related to the bolus progression that may be required to discern complex blood flow states properly, such as late-filling vessels in areas of severe stenoses, slow-filling vascular leaks, or relative filling patterns in complex vascular lesions (e.g., arteriovenous malforma-

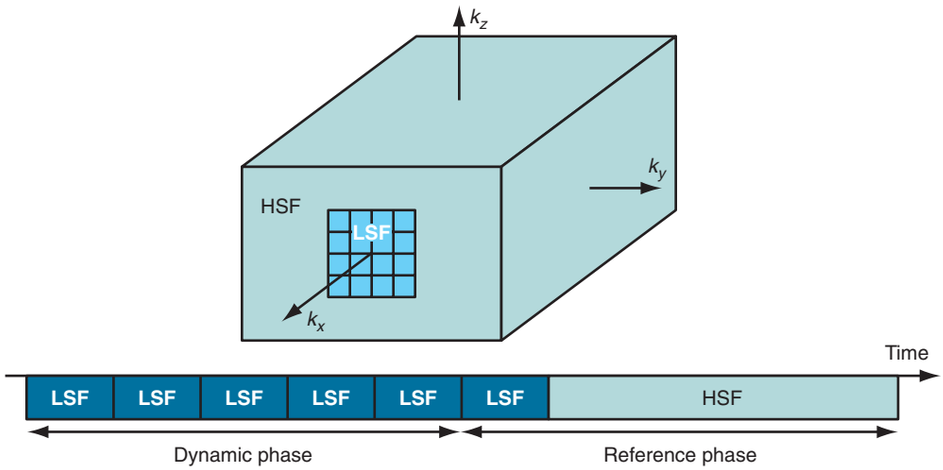

20 ■ **FIGURE 82-14** Dynamic CE-MRA with keyhole imaging. K-space is divided into a central k-space region representing the low spatial frequencies (LSF) and image contrast, and the high spatial frequencies (HSF) representing the image detail. To allow for higher frame rates, only the central region is updated during the dynamic phase, whereas the high spatial frequencies are only acquired once at the end of the scan. Dynamic images are reconstructed by updating the central k-space region.

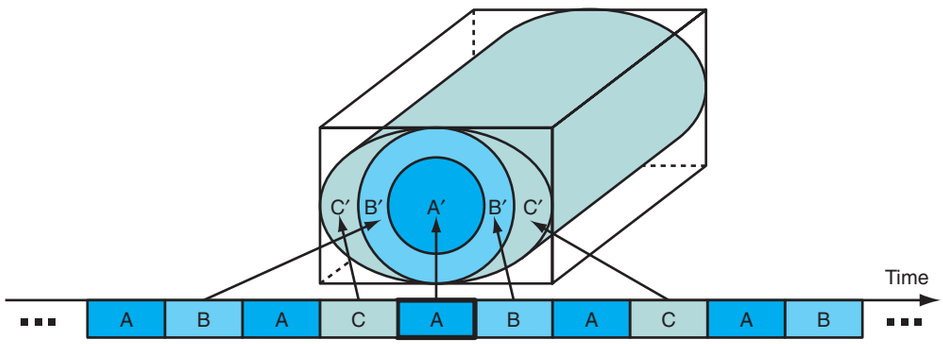

■ **FIGURE 82-15** Scheduling algorithm and data sharing scheme in three-dimensional TRICKS. The k-space regions are scheduled so that the central region, A, is acquired every other time frame, while the outer portions of k-space, B and C, are sampled less frequently. Information from the regions is shared for the reconstruction of image sets. In this example, the central region A′ of the reconstructed time frame is the actually acquired region, A, whereas regions B′ and C′ are linearly interpolated from adjacent regions.

tions). However, decreasing the scan time usually requires undesirable compromises in the spatial resolution. To facilitate dynamic acquisitions with high spatial resolution, data-sharing techniques are now commonly used.

In keyhole imaging, the acquisition process is split into a dynamic phase, in which central k-space data are acquired rapidly but with limited spatial resolution, and a subsequent second phase, whereby the missing high spatial frequency data (i.e., peripheral k-space data) is acquired to provide image detail.[18,19] These two acquisitions are then combined to generate a dynamic series with high spatial and high temporal resolution by updating only the central k-space region (Fig. 82-14). The underlying assumption is that most of the signal changes are reflected in the central k-space region (see Fig. 82-4). The drawback of the approach is the missing dynamic information about high spatial frequencies. Dynamic information is only captured with low spatial resolution whereas the high spatial frequency data, which define finer structures such as smaller vessels, are acquired only once and shared across the acquisition. If the relevant information under investigation contains changes in the outer portions of k-space, then keyhole imaging can produce images with an erroneous time course.[20]

Another commercially available approach, three-dimensional TRICKS, also shares data among time frames but does not update the central region only. In three-dimensional TRICKS (three-dimensional ***t***ime-***r***esolved ***i***maging of ***c***ontrast ***k***inetic***s***) imaging,[21] k-space is divided into subvolumes based on their distance to the center of k-space. Figure 82-15 shows an implementation of TRICKS with an elliptical centric view ordering scheme whereby the phase- and slice-encode ordering is based on their distance in the k_y-k_z plane from the center of k-space. In this figure, the subvolumes consist of a cylinder for the region containing lower spatial frequencies (A) and cylindrical shells of equal volume for the regions representing higher spatial frequencies (B and C). In practice, most examinations are acquired with a decreased spatial resolution in the slice-encoding direction, z, for a decreased imaging time and higher SNR. In this case, the higher spatial frequency regions become incomplete cylindrical shells. The central region, A, contains the low spatial frequency information and is sampled every second time

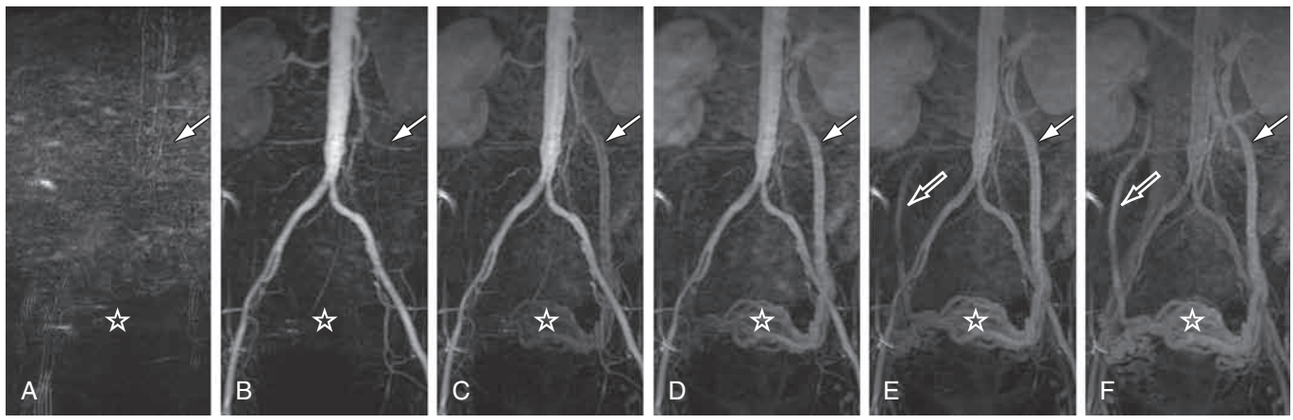

■ **FIGURE 82-16** Abdominal-pelvic three-dimensional CE-MRA with TRICKS demonstrates an enlarged left gonadal vein (**C-F,** *solid arrows*) and a plexus of parauterine varices (**C-F.** *asterisks*), consistent with pelvic congestion syndrome. The MIP images of several time frames reveal a clear separation of the arterial and venous phase and also show that the right gonadal vein (**E, F,** *arrows*) is filled significantly later.

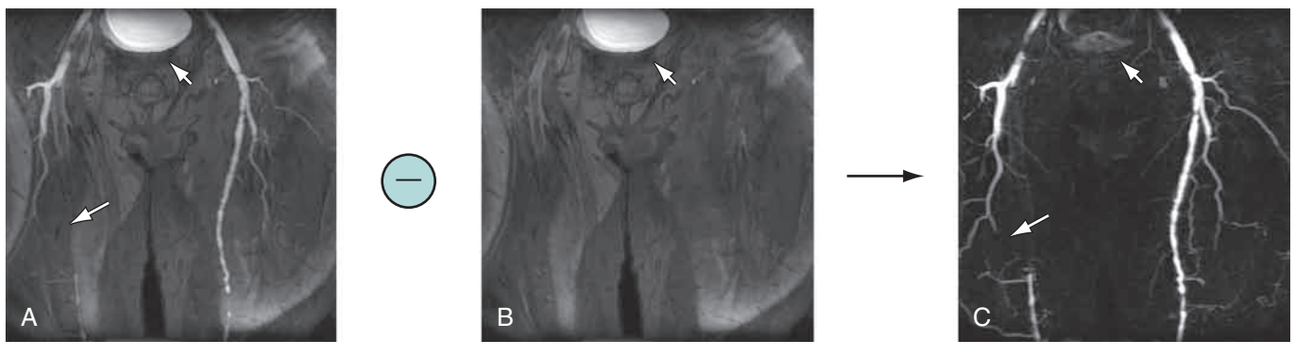

■ **FIGURE 82-17** Mask mode subtraction for a three-dimensional MR DSA exam of the pelvis showing an occlusion of the right femoral artery (*arrow*). **A,** MIP image of peak arterial enhancement. **B,** MIP image from a precontrast mask. **C,** Obtained by subtracting **B** from **A** on a slice-by-slice basis. As a result, stationary background noise from tissue and accumulation of contrast agent from an earlier injection, such as a signal in the urinary bladder (*asterisks*), is removed. Delineation of the vessels from the background is significantly improved in the subtracted image. *(Courtesy of Dr. Frank R. Korosec, University of Wisconsin-Madison, Madison, Wis.)*

frame, whereas regions B and C are sampled every fourth time frame only. For each newly sampled k-space subvolume, a complete k-space volume is assembled by temporal interpolation of the adjacent subvolumes acquired before, during, and after the current time frame.

This approach continuously acquires data during the passage of the contrast agent and is relatively insensitive to variation in timing and shape of the contrast bolus. An example for an examination of the abdominal and pelvic vasculature is shown in Figure 82-16. The maximum intensity projection (MIP) images represent reformats of three-dimensional volumes reconstructed for each time frame.

Mask Mode Subtraction

CE-MRA examinations usually include the acquisition of a precontrast mask so that techniques similar to those of digital subtraction angiography can be incorporated into the image display. Subtraction of a precontrast mask increases the contrast in the image by suppressing stationary background signals. The images have to be subtracted prior to the calculation of the MIP images to reflect the properties in the three-dimensional data set. As a result, smaller vessel details can be identified.

Figure 82-17 shows an example of mask mode subtraction for an examination of the pelvis. Mask mode subtraction is extremely beneficial when using multiple injections of a Gd chelate contrast agent, because the accumulated effects of prior contrast administration can be minimized by the use of imaging subtraction. With this method, time-varying background signals caused by patient motion or motion of the gastrointestinal tract are not affected. Although the contrast in the images is improved by mask mode subtraction, the actual SNR is decreased by $\sqrt{2}$, because the noise of the two images is additive.

Time-of-Flight Magnetic Resonance Angiography

Image contrast in TOF MRA relies on the inflow of blood into the imaging slice so that the signal from moving blood is brighter than that from stationary tissue. Because TOF MRA is inflow-dependent, it is best suited for vascular territories that allow for slice orientations with pronounced inflow effects, such as the lower extremities or carotid arteries, which have straight vessel paths and little in-plane flow. As a non–CE-MRA technique, TOF MRA provides an alternative to CE-MRA in patients with

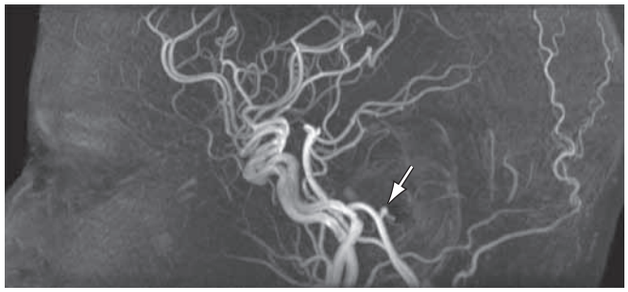

■ **FIGURE 82-18** MIP image of an intracranial TOF examination acquired at 3 T with submillimeter isotropic resolution reveals a 1-mm posterior inferior cerebellar artery (PICA) aneurysm (*arrow*) as an incidental finding in a 38-year-old female volunteer.

contraindications to Gd chelate contrast agents. It is routinely used for cranial MRA, providing spatial resolution and image quality superior to CE-MRA because the scan time is not limited to an arterial-venous window (Fig. 82-18). However, in vessels with more tortuous pathways with in-plane components and slow flow, TOF MRA acquisitions can suffer from disease-mimicking signal voids.

Two-Dimensional Time-of-Flight

The TOF acquisition strategy aims to saturate partially the longitudinal magnetization of nonmoving spins so that unaffected moving spins appear bright in comparison.[22] Similar to CE-MRA, a spoiled gradient echo sequence is used to achieve this goal. With this acquisition, the repeated RF pulses used for excitation in the beginning of each TR diminish the available longitudinal magnetization until an equilibrium between signal regrowth from relaxation and signal decrease from the RF excitation is reached (Fig. 82-19). The actual signal depends on the TR, the T1 of the tissue, and the flip angle. In two-dimensional TOF imaging, the imaging slice is oriented perpendicular to the flow direction. Stationary tissue experiences all RF pulses and will only have small signal contributions in the resulting image. However, only a few RF excitations will affect flowing blood as it enters the imaging slice, resulting in a relatively high signal contribution in the angiogram. The longer the blood stays in the imaging slice, the more the signal differences diminish. Consequently, the vessel to background contrast decreases as the slice thickness increases or the velocity of blood flow decreases. A longer TR will increase the vascular signal but will also increase the signal from background tissues and lengthen the scan time. Therefore, intermediate TR times are usually chosen. An increased flip angle will decrease the signal contribution from stationary tissues, but signal from blood that undergoes multiple RF excitations will also decrease (see Fig. 82-19). Therefore, intermediate flip angles are used for most clinical applications.

Without any further modifications, arterial and venous blood flow will cause a bright signal in TOF angiograms. In most applications, it is desirable to image selectively the arteries or veins only. This can be easily achieved with the use of saturation bands in vascular regions with arterial and venous flow in opposing directions.[23] With this approach, a saturation pulse is applied parallel to the

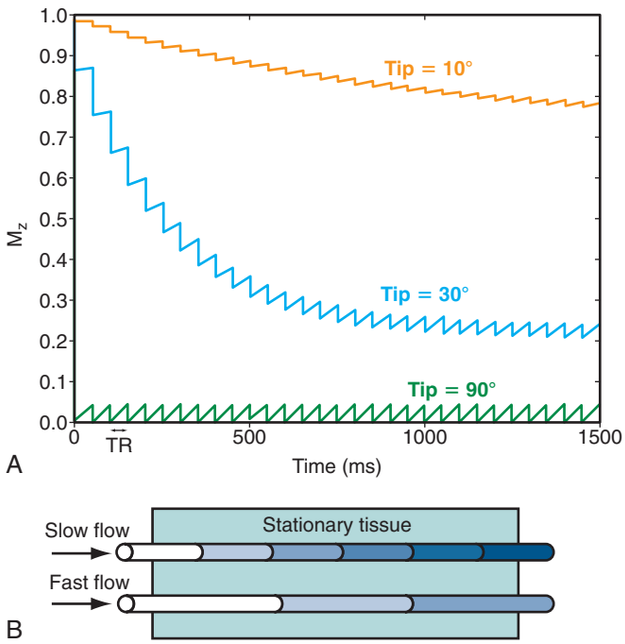

■ **FIGURE 82-19** Contrast mechanism in TOF MRA. **A,** Repeated RF excitations decrease the longitudinal magnetization (Mz) until the regrowth during each TR equals the decrease from the excitation pulse. The signal behavior depends on the T1 (here, 1200 ms), flip angle (varied from 10 to 30 degrees and 90 degrees), and TR time (here, 50 ms). **B,** Higher contrast for fast-flowing blood that experiences fewer RF excitations in the imaging slice or volume as compared with slower flowing blood that can suffer from partial saturation effects.

imaging slice to eliminate unwanted inflow signal from a particular direction. Figure 82-20 demonstrates an example of arterial and venous suppression in an axial slice through the neck with the use of superior and inferior saturation slabs.

Volume data can be achieved with two-dimensional TOF MRA whereby a series of contiguous two-dimensional slices are acquired sequentially over the vascular territory of interest. In most cases, two-dimensional TOF MRA is accompanied by a saturation band (e.g., inferior saturation band for lower extremity arterial imaging) that is applied sequentially with each two-dimensional slice, a feature also known as a walking saturation band. This approach is commonly used in TOF examination of the lower extremities, in which coverage of the vessels from the pelvis to the feet is achieved with sets of axial slices that are acquired over multiple stations (Fig. 82-21). TOF examinations in the abdomen, pelvis, and lower extremities typically have to be cardiac-gated because of the flow pulsatility that can result in significant fluctuations in arterial signal and artifacts. The acquisition of central k-space data during systole optimizes arterial inflow signal on TOF MRA.

Disadvantages of two-dimensional TOF acquisitions include the relatively long acquisition times, which reduce patient comfort and increase the likelihood for bulk patient motion artifacts. Because temporary motion might only affect a single slice, this could result in a focal decreased signal and mimic the appearance of vascular disease, such as stenosis. Moreover, the relatively thick

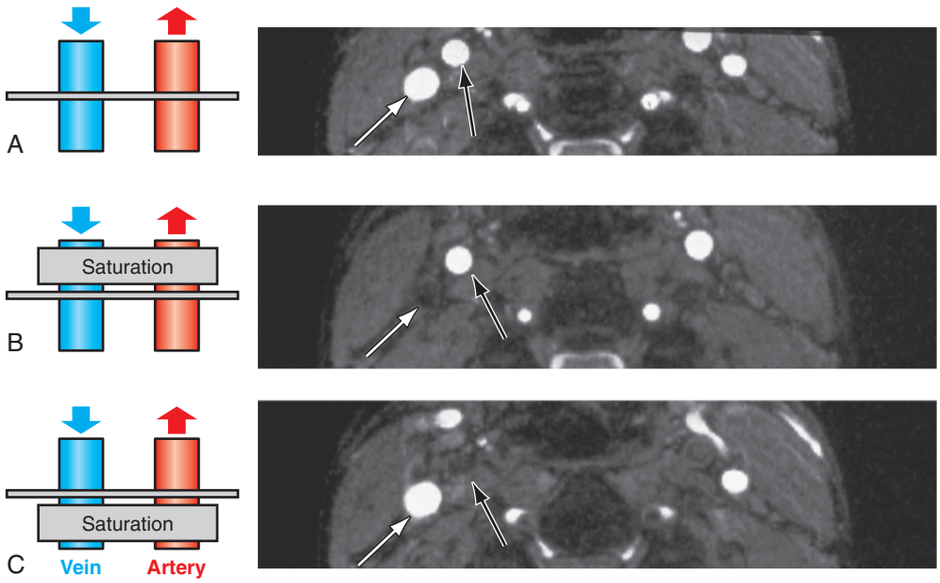

■ **FIGURE 82-20** Inflow effect and the use of saturation slabs in TOF MRA to tailor the image characteristics to the desired anatomic information. **A,** With no saturation slab, venous and arterial inflow, such as from the carotid artery (*open arrow*) and jugular vein (*solid arrow*) contribute to the signal in the axial slice through the neck. **B,** When placing a saturation slab superior to the imaging slice, the magnetization of the inflowing venous blood will be saturated and the arterial signal will dominate the image. **C,** A saturation slab placed inferior to the imaging slide causes the opposite effect, with suppression of the arterial signal and a bright venous signal.

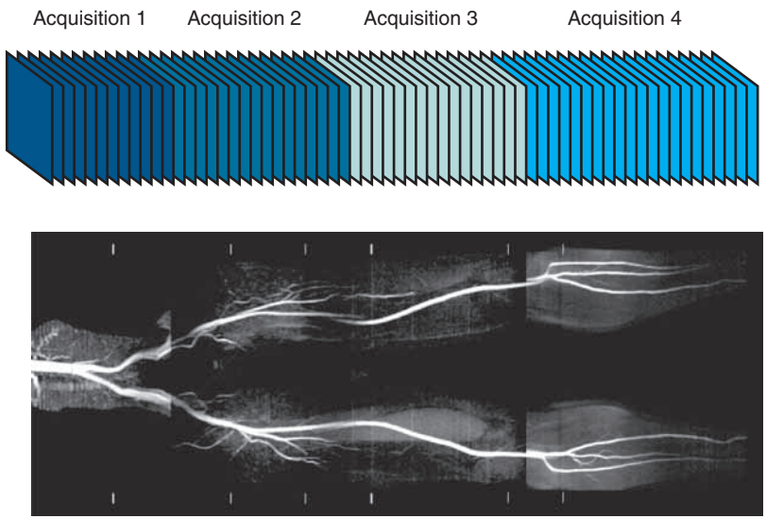

■ **FIGURE 82-21** Sequential two-dimensional TOF examination of the lower extremities. The scan is completed in four separate acquisitions because of the limited field of view for an MR image free of geometric distortions. Multiple axial slices are acquired at each of the four stations and displayed as a coronal MIP image.

slices and longer TE associated with two-dimensional TOF imaging can further contribute to signal loss in areas of complex flow, such as downstream of a stenosis, or areas of irregular luminal geometry, such as with atherosclerotic plaque. All these lead to a tendency to underestimate luminal diameter and to possible overestimation of a stenosis to the point of even simulating an arterial occlusion. However, two-dimensional TOF may serve as a good screening method for the presence of vascular disease in vascular territories such as the carotid arteries.

Three-Dimensional Time-of-Flight

In three-dimensional TOF MRA,[24] the SNR is improved compared with sequential two-dimensional TOF because all the magnetization in the excited volume contributes to the signal of each sampled data point. In addition, the slice encoding for thin slices less than 1 mm thick, with reasonable echo times for artifact suppression, poses major challenges to two-dimensional TOF but can easily be achieved with three-dimensional TOF. The phase-encodings steps and not the slice-encoding gradient determine the slice thickness in three-dimensional TOF. The increased spatial resolution reduces intravoxel dephasing and permits the visualization of smaller vessels that otherwise might be obscured by partial voluming effects.

The drawback of three-dimensional TOF is the reduction in the inflow effect because the moving blood remains longer in the imaging volume and experiences more RF excitations. The flip angle is reduced (<30 degrees) to preserve signal contributions from slower moving blood. However, signal from stationary tissue is also increased and leads to diminished vessel contrast.

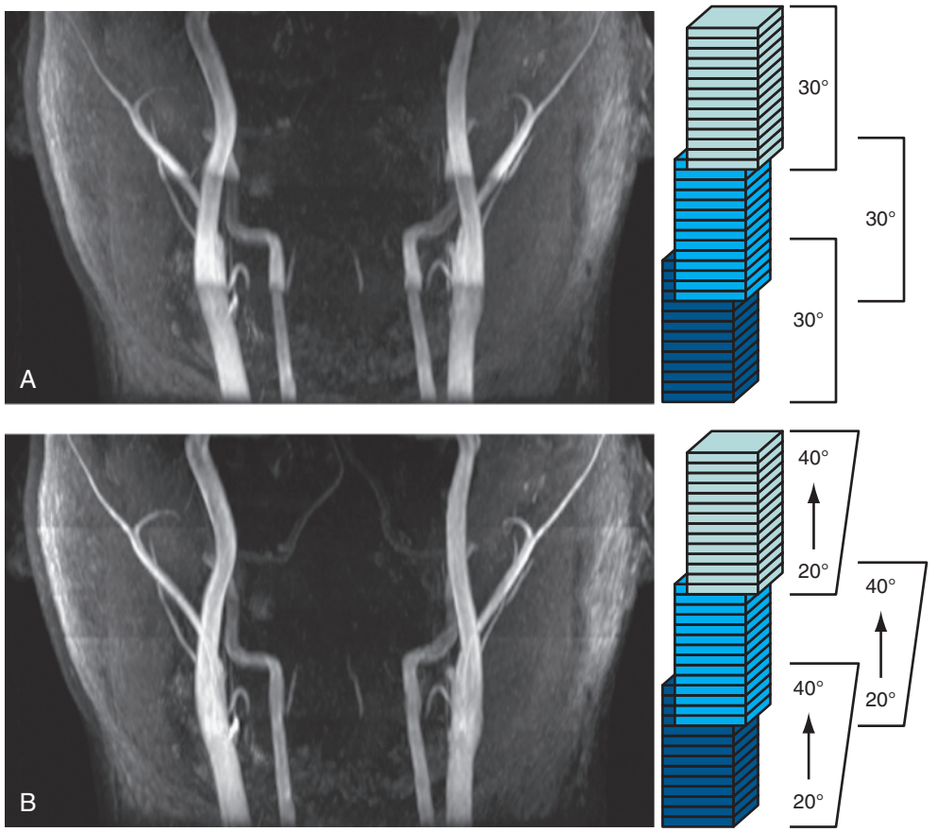

■ **FIGURE 82-22** Volumetric TOF acquisition with MOTSA (multiple overlapping thin slab angiography).[24] This neck examination was acquired with three partially overlapping thin slabs to provide large coverage with thin slices, high SNR, and good vessel contrast. **A,** When a constant flip angle of 30 degrees is used, the vessel signal decreases as the arterial blood travels supine and experiences additional RF pulses (*arrows*). **B,** The homogeneity of the vessel signal can be further improved with ramped flip angles to counteract this effect. *(Courtesy of Dr. Frank R. Korosec, University of Wisconsin-Madison, Madison, Wis.)*

Sequential Three-Dimensional Time-of-Flight

The signal loss of flowing blood from saturation in a thick three-dimensional volume can be reduced by exciting smaller volumes. The use of MOTSA (multiple overlapping thin slab angiography)[25] provides large coverage with thin slabs (i.e., thin volumes), thereby combining benefits from two-dimensional (reduced blood saturation) and three-dimensional TOF (small voxels, high SNR, and short TE). Overlapping of the thin slabs reduces artifacts from slab profiles and partial saturation, making this approach the method of choice for cranial and carotid MRA, in which high spatial resolution is essential (Fig. 82-22A; see Figs. 82-7 and 82-18). Such volumetric acquisitions benefit from ramped flip angles designed to counteract the signal loss from partial saturation effects when blood moves through the imaging volume. A lower flip angle, in which the arterial blood enters the imaging volume, and a higher flip angle, in which the arterial blood leaves the imaging slice, provide a homogeneous vessel signal across the imaging volume (see Fig. 82-22B). The linearly varying flip angle reduces saturation effects for the blood entering the volume and increases the signal for the blood leaving the volume. The amplified saturation of blood exiting the volume is inconsequential because it will not be used for signal generation once it has left the imaging volume.

Phase Contrast Magnetic Resonance Angiography

Phase contrast MRA (PC MRA) provides quantitative velocity and flow measurements in vascular territories throughout the body and, like TOF, can be acquired in two-dimensional or three-dimensional modes. Two-dimensional PC MRA is commonly used in an ECG-gated cine mode for the dynamic assessment of cardiac valve function, pulmonary and systemic flow, and unusual shunt determinations in patients with congenital heart disease. In addition, MR angiograms can be derived from the acquired data, making this approach another alternative to CE-MRA in patients who cannot be given Gd chelate contrast agents. PC MRA works well for two-dimensional projections through thick sections and, compared with TOF methods, smaller vessels with low blood velocities can be identified. PC MRA is also particularly good when performed following the administration of Gd chelate contrast agents and is a good alternative when the initial CE-MRA scan is nondiagnostic.[26]

Whereas the imaging contrast between blood and surrounding tissues in all other MRA techniques is based on the magnitude of the magnetization, PC MRA uses bipolar gradients for phase manipulation of the magnetization.[27] Figure 82-23 demonstrates how the gradient pair causes the phase of stationary spins to accumulate to zero,

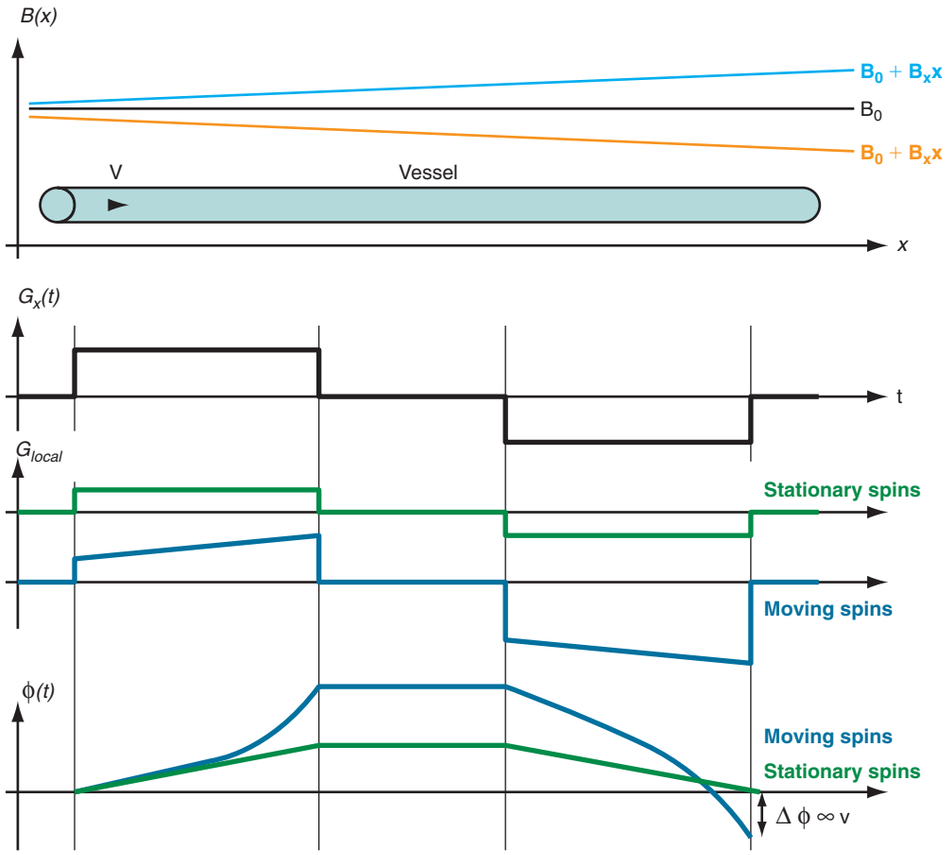

■ **FIGURE 82-23** Velocity encoding in PC MRI. A field gradient, G_x, is applied along a direction, here shown for the x-axis. The gradient is switched on and off in the shape of a bipolar gradient with a positive and negative lobe, $G_x(t)$.Stationary tissue experiences a positive and negative magnetic field superimposed to the stationary field B_0, resulting in a zero phase from a faster and slower precession at the end of the bipolar gradient. Blood that moves along the direction of the gradient experiences a verying field while the bipolar gradient is switched on. The resulting net phase, $\Delta\varphi$, is proportional to the velocity, v.

whereas spins that move along the axis of the gradient accumulate a net phase proportional to their velocity. Because MR images contain unpredictable phase contributions from magnetic susceptibilities, eddy currents, measurement imperfections, and other sources, a reference image without velocity encoding has to be acquired. On subtraction of the reference phase from the velocity-encoded image, these local phase offsets are removed. Therefore, one-directional velocity encoding requires the acquisition of two images, thereby doubling the scan time. In the phase difference image, the signal in each voxel is linearly proportional to its velocity. Blood moving along one direction of the gradient axis is assigned a bright (white) signal and blood moving along the opposite direction is assigned a dark (black) signal. PC acquisitions, therefore, can provide directional information of blood flow. A magnitude image is also reconstructed as the average of the two acquisitions to provide anatomic information. The velocity-encoding direction can be perpendicular to the imaging plane (through-plane flow) or in plane in the phase or frequency direction. For pulsatile flow measurements, cine PC imaging with ECG gating[28] is performed to capture the flow dynamics for multiple time points within the cardiac cycle. Because of the slower acquisition speed of MRI , data sampling for cine series stretches over multiple heartbeats. Reductions in scan time because of high-performing gradients (shorter TR) and parallel imaging can improve the temporal and spatial resolution achievable for cine PC imaging within a patient-friendly breath-hold duration. Figure 82-24 shows a magnitude image and several phase difference images at peak systolic flow for an oblique imaging plane in a chest that was oriented perpendicularly to the path of the ascending aorta with through-plane velocity encoding. 14

The application of bipolar gradients along a second and third gradient axis extends the technique to two-dimensional and three-dimensional flow encoding. The same reference image can be used for calculating the directional phase differences, yet the total scan time is prolonged to three or four acquisitions, respectively. Figure 82-25 shows an example of three-directional velocity encoding for a slice covering the aortic arch. The different in-plane and through-plane components of the velocity vector can be appreciated as three gray-scale images. The concept can be further extended to volumetric cine imaging,[29] thereby providing comprehensive information on the anatomy and velocity fields over a vascular territory.

One important parameter in PC MR is the proper choice of the velocity-encoding setting. The velocity of a voxel is determined by its phase accumulation while the bipolar gradient waveform is played out. Because the phase is a cyclic entity, there is a maximum and a minimum phase indistinguishable from a wrapped phase. For example, a precession of +190 and −270 degrees results in the same final position on the unit circle. Because the precession path to the final position is unknown in PC

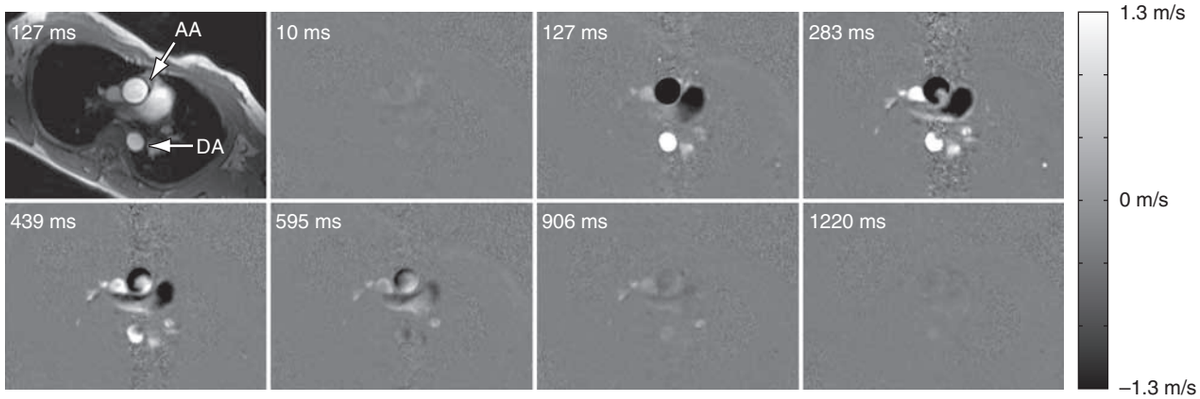

■ **FIGURE 82-24** Two-dimensional cine phase contrast MR with through-plane velocity encoding. The imaging slice for the velocity-encoded acquisition was placed perpendicular to the orientation of the ascending aorta (AA). The magnitude image and the selected seven cine frames from the velocity-encoded velocity images show the ascending and descending aorta (DA). The gray-scale intensity is proportional to the velocity in each voxel, with dark values indicating flow in the inferior to superior direction and bright voxels indicating flow in the opposite direction.

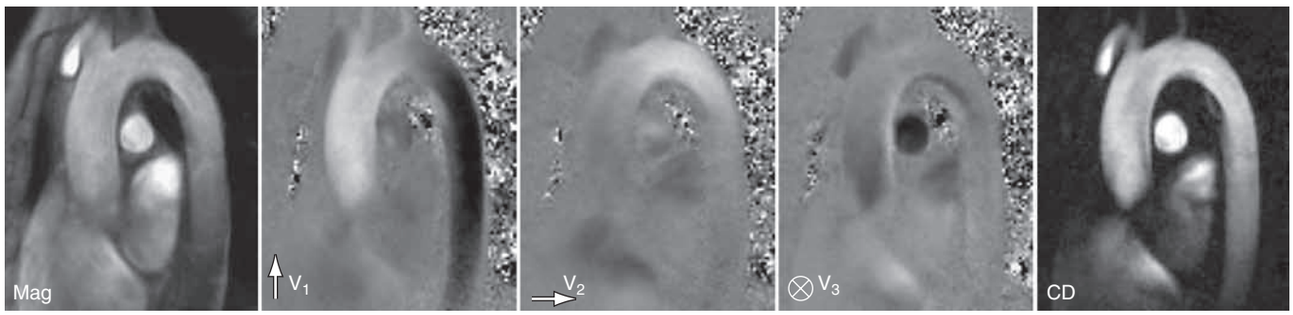

■ **FIGURE 82-25** PC MRA with three-directional flow encoding. The imaging slice was oriented along the orientation of the aortic arch and shows a single time frame of a three-directional cine acquisition. CD, complex difference image as an angiogram that shows vessel anatomy only based on the three velocity components, but without quantitative information; Mag, magnitude image; v_1, velocity component in the inferior to superior in-plane direction; v_2, velocity component in the anterior to posterior in-plane direction; v_3, velocity component in the left to right direction (through-plane).

MR, only phase precessions less than +180 or −80 degrees can be uniquely identified with the proper velocity. The velocity corresponding to a 180-degree phase is referred to as the velocity-encoding parameter (Venc) of the acquisition and has to be carefully adjusted to the imaging task. If chosen too low, velocity aliasing from phase wrap will occur, which can result in a heterogeneous signal within the vessel (and inaccurate flow measurements if flow quantification is performed). If chosen too high, the phase difference data will have a small signal range and a decreased velocity-to-noise-ratio (VNR), secondary to a higher noise floor. Venc is determined by the shape of the bipolar gradient waveform.

Figure 82-26 shows an example of an axial imaging slice in the neck with optimized Venc settings for arterial flow analysis (50 cm/sec) and cerebrospinal fluid (CSF) flow analysis (5 cm/sec) and an intermittent Venc of 30 cm/sec. In practice, the bipolar gradient waveform is automatically calculated from a user input on the desired Venc based on reference velocities for normal vessels or expected velocity ranges. Ideally, the Venc is set slightly above the peak velocity within the vessel of interest. However, peak velocity, especially in diseased vessels, may be difficult to predict, and the PC acquisition may need to be repeated at a more appropriate Venc setting if the initial Venc setting is suboptimal.

Several factors lead to an increased susceptibility of PC MR to intravoxel dephasing:

1. The presence of velocity-encoding gradients increases the minimum TE, which in turn allows more intravoxel dephasing from all sources, including magnetic susceptibility.
2. Voxels that contain heterogeneous velocity components will have a decreased net phase. This is a common occurrence in areas of disturbed flow. Again, the longer the TE, the more pronounced the effects become. The artifacts can be reduced by minimizing the TE (e.g., by using fractional echo acquisitions and high-performance gradients) and by decreasing the voxel size.
3. The imaging gradients themselves cause intravoxel dephasing while spins move during their application. Gradient moment nulling[30] is used to reduce these effects but also further lengthens the TE.

Postprocessing

In addition to the magnitude and phase image, complex difference (CD) images can be derived from PC acquisitions. The complex difference image is obtained as the length of the vector obtained by complex subtraction of the velocity-encoded data from the reference data, thereby

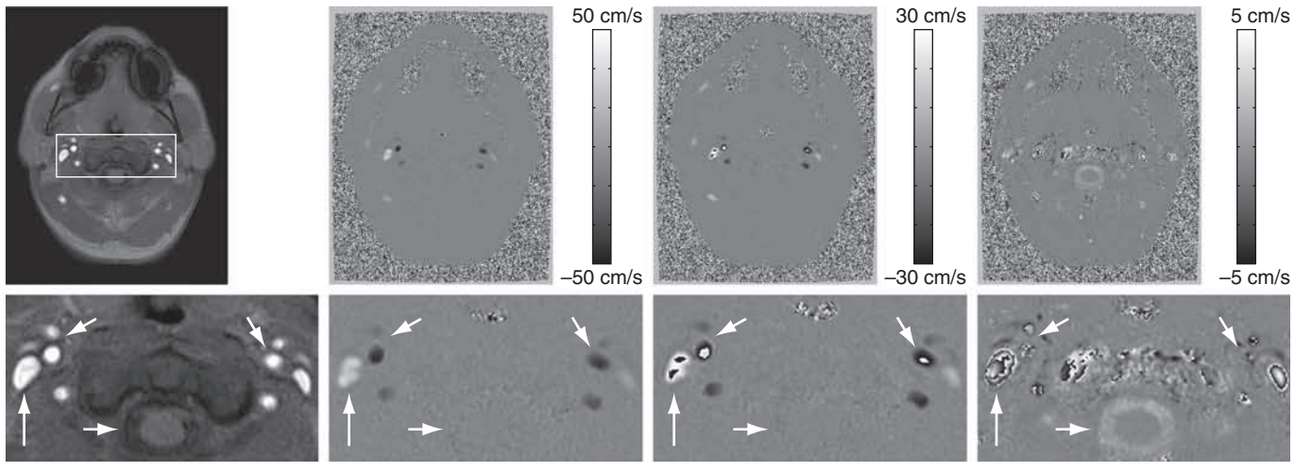

■ **FIGURE 82-26** Two-dimensional PC measurements with velocity aliasing. This axial cine PC series was acquired at the neck of a healthy volunteer with Venc settings of ±50, ±30, and ±5 cm/s. With a venc of ±50 cm/s, the flow through the carotid artery (*small arrows*) and the jugular vein (*long arrows*) remains artifact-free because all velocities in the imaging slice are within the encoded velocity range. If the Venc is reduced to 30 cm/s, then velocity aliasing occurs in the carotid arteries and the right jugular vein during peak systolic flow. If the Venc is reduced further, severe aliasing occurs in almost all vessels, but the velocities of the slow-flowing CSF (*bold arrows*) can be quantified while it is hidden in the noise level with the higher Venc acquisitions.

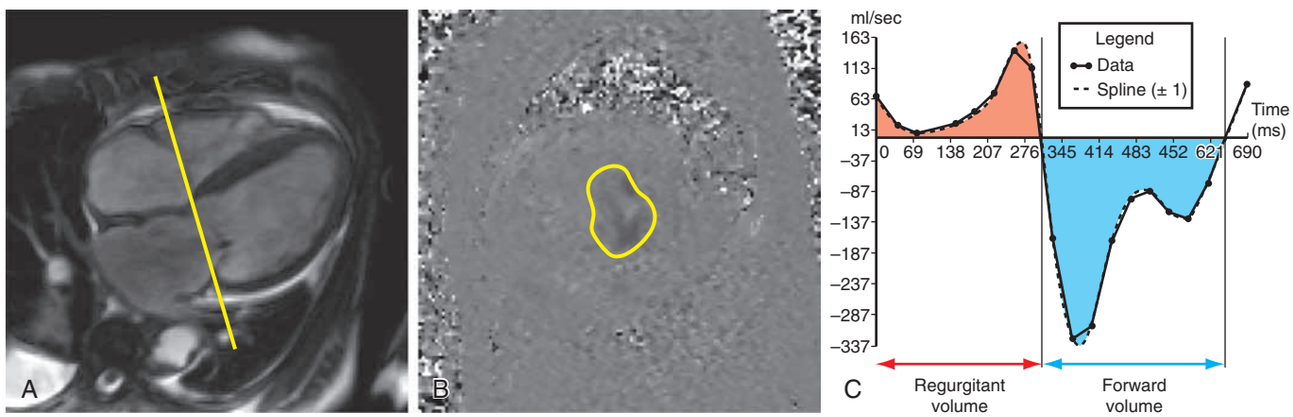

■ **FIGURE 82-27** Flow analysis from PC MRA images across the cardiac valves. **A,** The four-chamber balanced SSFP image is used for localization of the valve plane (*yellow line*). **B,** The regurgitant jet is used to prescribe the phase contrast acquisition perpendicular to the jet. A manually drawn region of interest delineates the area from which the desired flow information is obtained. **C,** The areas over and under the flow curve as a function of time determine the regurgitant volume (*red area*) and forward volume (*blue area*). *(Courtesy of Dr. C. Francois, University of Wisconsin-Madison, Madison, Wis.)*

incorporating phase and magnitude into the calculation. As opposed to phase difference images, complex difference images are non-negative and do not suffer from discontinuities from velocity aliasing. As shown in Figure 82-25, they are well suited for the display of vessel paths with good background suppression, but do not provide quantitative or directional flow information.

Flow quantification is performed with software packages that allow for the interactive definition of regions of interests (ROIs). In a two-dimensional image with through-plane velocity encoding, the volume flow rate through a voxel is calculated as

$$Q_{voxel} = \text{velocity} \times \text{area}$$

where Q_{voxel} is given in mL/min, velocity is determined using the phase map images (cm/sec), and area is given by the spatial resolution of the phase map (cm^2). The flow rate through a vessel is simply determined by integration over a manually or semiautomatically defined cross-sectional ROI that encompasses the vessel circumference. Flow volumes throughout the cardiac cycle can be calculated by integration over the sampled time points, as shown in the valve analysis in Figure 82-27.

Flow analysis and visualization for cine three-directional volumetric velocity mapping has gained significant interest but is currently limited to research applications, partly because of the lack of intuitive analysis platforms. Advanced visualization techniques such as particle tracers, streamlines, and velocity vectors are limited to specialized software platforms (Fig. 82-28). However, the availability of comprehensive information on cardiovascular anatomy and function from a single examination is appealing and possibly allows for the derivation of additional hemodynamic parameters, such as trans-stenotic pressure gradi-

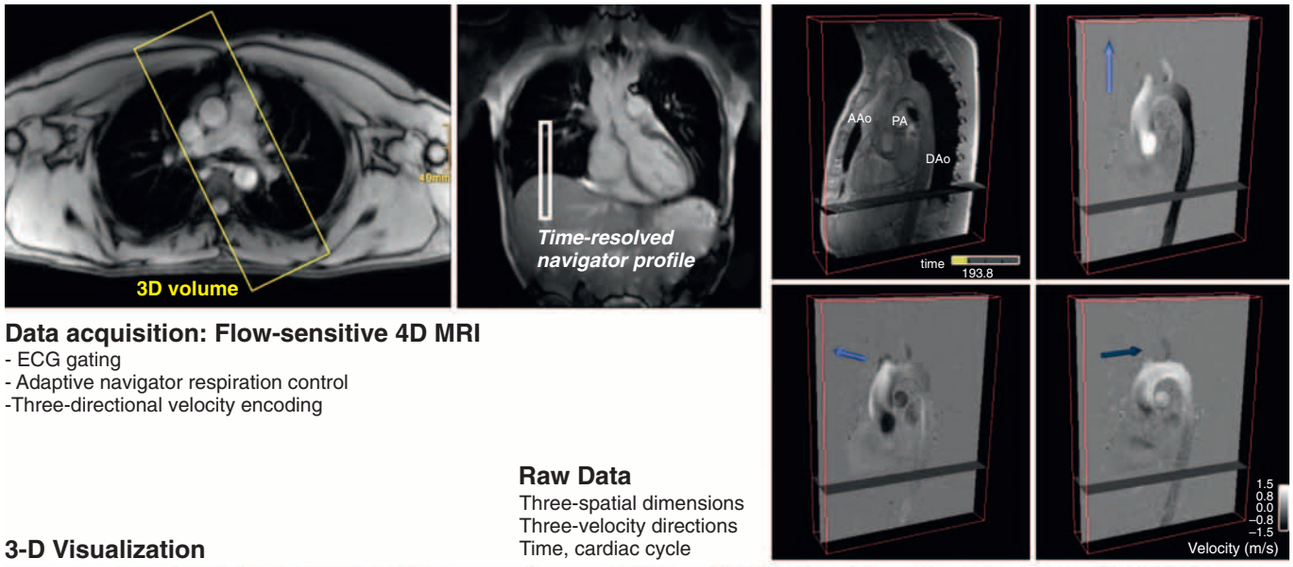

Data acquisition: Flow-sensitive 4D MRI
- ECG gating
- Adaptive navigator respiration control
-Three-directional velocity encoding

Raw Data
Three-spatial dimensions
Three-velocity directions
Time, cardiac cycle

3-D Visualization

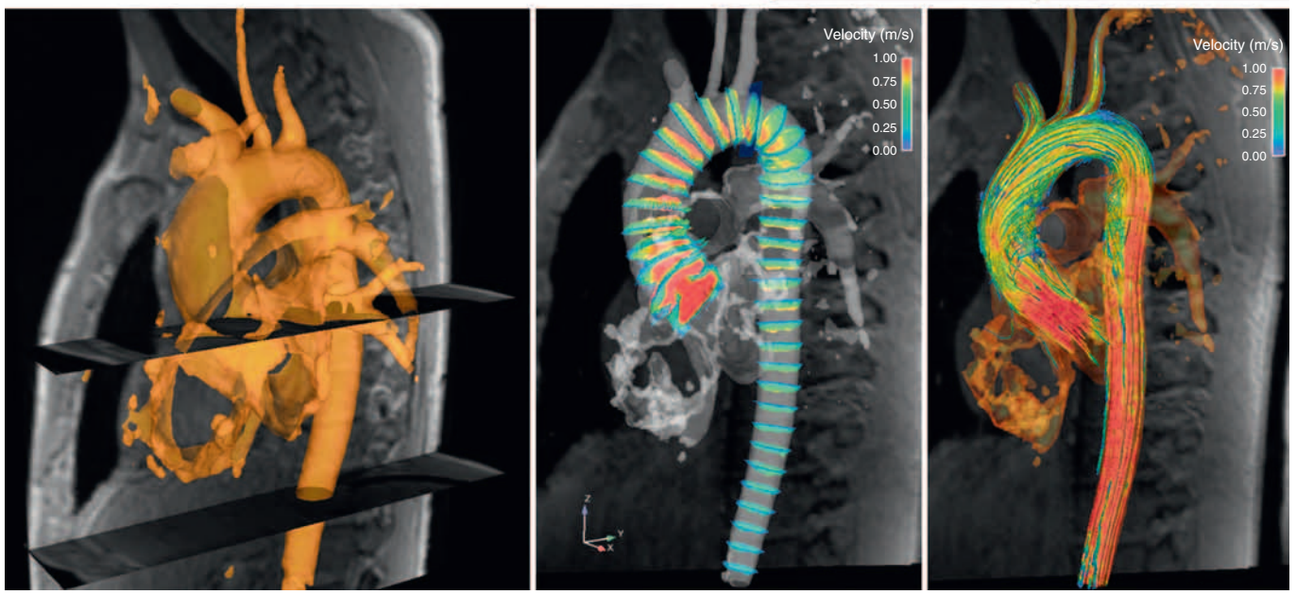

3D PC-MRA **Velocity profiles** **3D stream lines**

■ **FIGURE 82-28** Flow-sensitive four-dimensional (4D) MRI provides volumetric, three-directional, cine PC measurements. The acquisition allows for the capture of complex hemodynamic and postprocessing with advanced visualization software and the derivation of additional hemodynamic parameters. This acquisition uses a navigator signal for respiratory gating of the lung/liver tissue interface. *(Courtesy of Dr. Michael Markl, University Hospital. Freiburg, Germany.)*

ents and wall shear stress within the limits of the spatial resolution of the acquisition. Without taking advantage of accelerated imaging methods, the total scan time for such measurements, T_{scan}, becomes prohibitively long:

$$T_{scan} = (N_{FD} + 1) \times N_{PE} \times N_{SE} \times T_R \times T_{cp}$$

where N_{FD} = no. of flow-encoding directions, N_{PE} = no. of phase-encoding directions, N_{SE} = no. of slice-encoding directions, T_R = repetition time, and $T_{R\,=}$ no. of cardiac phases. Similar to CE-MRA, accelerated PC imaging approaches include partial Fourier acquisitions, view sharing and temporal interpolation schemes, and use of parallel imaging techniques.

Steady-State Free Precession Magnetic Resonance Angiography

In balanced steady-state free precession (SSFP) imaging, the magnetization is manipulated so that both the transverse and the longitudinal components reach a steady state and contribute to the MR signal. The clinical adaptation of this imaging approach, also known as true fast imaging with steady-state precession (trueFISP), fast imaging employing steady-state acquisition (FIESTA), and balanced fast field echo (bFFE), had been delayed until recent hardware improvements, particularly in gradient performance and field shimming, minimized, image-degrading artifacts. This sequence is extensively used for the evaluation of cardiac function.[31]

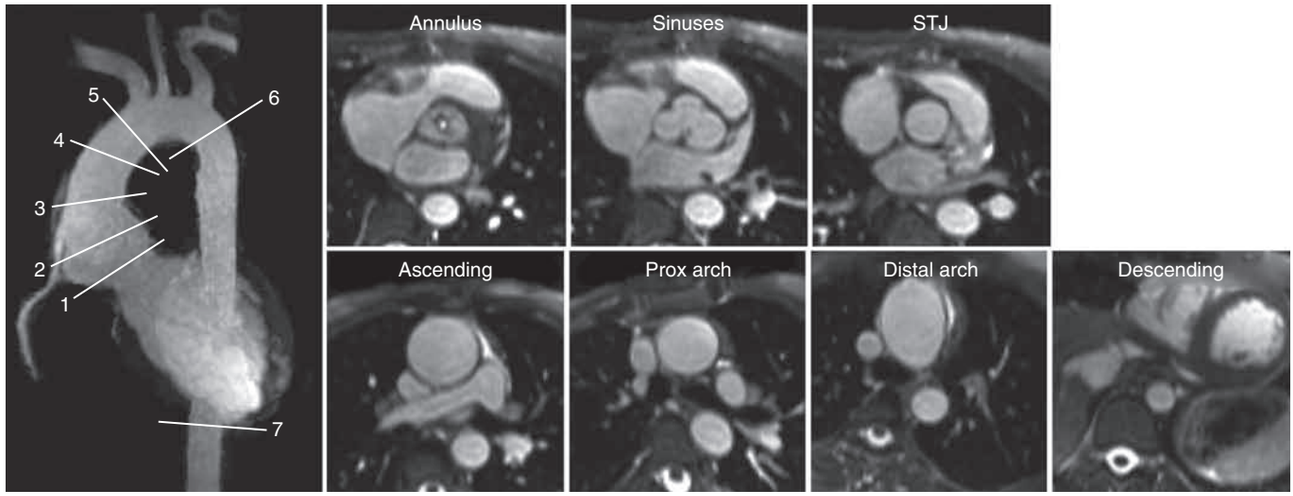

■ **FIGURE 82-29** Images obtaoned with bSSFP MRA of the thoracic aorta in a patient with a dilated aortic root. The volume-rendered image (*left*) demonstrates the large coverage of the acquisition. Multiplanar reformats of the source images are shown at seven levels (1-7) and provide high signal from blood because of the T2 over T1 contrast. Fat suppression was used in the ECG-gated sequence. *(Courtesy of Dr. C. Francois, University of Wisconsin-Madison, Madison, Wis.)*

Whereas the image contrast in the rapid spoiled gradient echo sequence depends mostly on T1-dependent and inflow effects for a high blood signal, SSFP provides an inherently high steady-state signal for species with a large T2/T1 ratio, such as in blood. This property explains its extensive use in the evaluation of cardiac function, with striking contrast between the blood pool and the myocardium. However, not only blood has a large T2/T1 ratio, and the challenge for SSFP MRA applications becomes the suppression of unwanted signals, particularly from fat and veins. Fat suppression is usually accomplished with water-selective excitation pulses or repeated spectral fat saturation pulses. Figure 82-29 shows MRA scans of the thoracic aorta acquired with an SSFP sequence and fat suppression.

In SSFP MRA, data are acquired with very short TR times (~3 ms), allowing for breath-held ECG-gated acquisitions. This approach is becoming a promising alternative for patients with contraindications to CE-MRA with Gd chelate contrast agents. Several modified acquisition schemes have been suggested to improve signal suppression from fat and veins, including the use of arterial spin labeling or saturation bands similar to the ones used in TOF imaging for the suppression of venous signal and slab-selective spin inversions.[2] Future clinical evaluations are needed to assess their reliability over a broad patient base. It must also be noted that signal on SSFP MRA is good after the administration of Gd chelate contrast agents and provides an additional imaging option following CE-MRA if specific regions need reassessment.[32]

Black Blood Imaging

One final technique, black blood imaging, requires specific mention, because it also can be used for the depiction of blood vessels. With black blood imaging techniques, the stationary tissue produces a signal with high amplitude whereas the signal from moving spins is nulled.[33] This is the reverse of all other MRA techniques described here, which result in bright vascular signals. Black blood methods are based on spin-echo sequences with long TR times. The most common approach for generating this contrast is by the use of a black blood pulse consisting of two consecutive 180-degree excitation pulses (double-inversion recovery fast spin echo [DIR FSE]). The first pulse is a non–slice-selective pulse that effectively inverts the magnetization in the excitation volume of the transmit coil. As a result, the initial value of the normalized longitudinal magnetization is not 0, as is the case for a 90-degree excitation, but −1. The second pulse is selective to the magnetization of protons in the imaging slice, basically reversing the previous inversion. However, the protons outside the imaging slice are not affected by the second inversion pulse. Therefore, they undergo T1 relaxation to return to their equilibrium state (Fig. 82-30). The magnetization of blood entering the imaging slice will undergo the same relaxation and its image signal can be nulled when the data acquisition is synchronized with the zero crossing of the longitudinal magnetization. The acquisitions are usually based on fast spin-echo sequences with cardiac gating to allow for imaging with long TRs, ensuring the proper regrowth of the longitudinal magnetization prior to the next excitation.

Black blood imaging is of value whenever high contrast between the vessel lumen and vessel wall is desired and is typically performed as a two-dimensional acquisition. This technique is particularly useful for imaging atherosclerotic plaque, vasculitis, coronary arteries, and cardiac and intravascular masses and clots (see Fig. 82-30). Furthermore, non–contrast-enhanced MRA sequences that rely on bright blood signal can suffer from signal dephasing in areas of complex flow, resulting in the overestimation of stenoses. Black blood sequences do not suffer from this artifact because the acquisition is designed to provide no signal from within the lumen and can serve as a good adjunct to bright blood MRA for vascular diagnosis. However, drawbacks of this approach include insufficient contrast in regions with low signal intensity background, such as air and bone, and persistent signals in vessels with slow or recirculating blood.

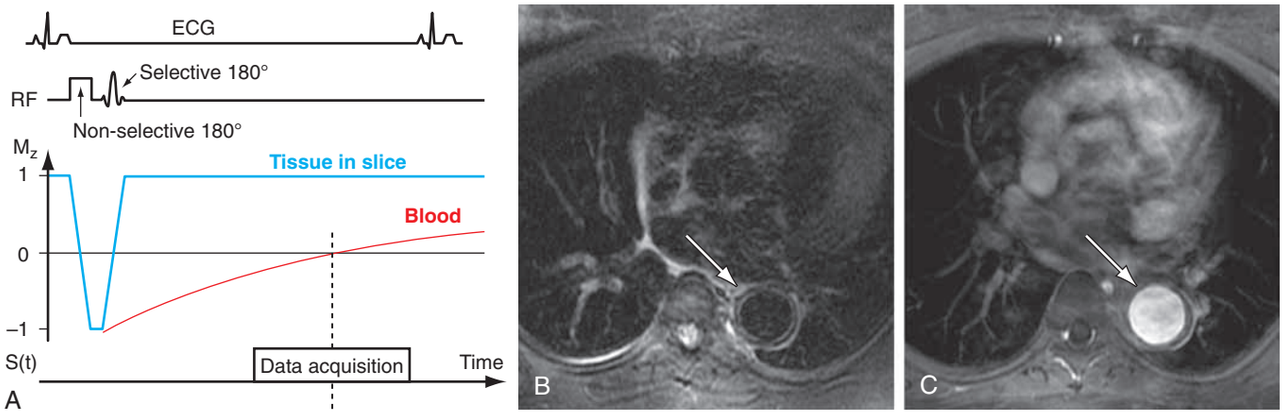

■ **FIGURE 82-30** Black blood MRA with double inversion pulse. **A,** The first 180-degree pulse is nonselective and excites all protons inside and outside the imaged slice. The second 180-degree pulse is slice-selective and inverts only the magnetization of protons within the slice. The protons in blood entering the imaging slice have undergone only the nonselective excitation and their longitudinal magnetization, M_z, undergoes T1 relaxation. The data acquisition is centered around the zero crossing of the blood magnetization to null the signal from blood in the resulting image. **B,** This is demonstrated in a patient with Takayasu arteritis in whom the aortic wall is thickened (*arrows*) and displays increased signal intensity in T2-weighted black blood images resembling those in aortitis. The hypointense signal of the blood provides a clear separation of the vessel wall and aortic lumen. **C,** For comparison, the corresponding T1-weighted image with fat saturation obtained after IV contrast injection is displayed.

KEY POINTS

- Various MR techniques (e.g., contrast enhancement, time-of-flight, phase contrast, black blood, steady-state free precession) that can provide illustration of blood vessels are available.
- Hardware developments, such as more rapid and stronger gradients systems and the availability of multicoil receiver systems, together with novel acquisition schemes such as parallel imaging, have led to significantly accelerated MRA scans.
- Optimized MRA protocol development requires an understanding of the tradeoffs regarding anatomic coverage, spatial and temporal resolution, and signal-to-noise ratio.
- Contrast-enhanced MRA is a widely used clinical technique that requires synchronization of the MRA image acquisition (notably the central k-space views) with the arrival of the contrast bolus into the target vascular bed.
- TOF MRA relies on the inflow effect of flowing blood and is best suited for vessels with relatively straight trajectories, such as the carotid arteries or peripheral arteries.
- Phase contrast MRA can provide quantitative flow measurements and directional information.

SUGGESTED READINGS

Larkman DJ, Nunes RG. Parallel magnetic resonance imaging. Phys Med Biol 2007; 52:R15-R55.

Lotz J, Meier C, Leppert A, Galanski M. Cardiovascular flow measurement with phase-contrast MR imaging: basic facts and implementation. Radiographics 2002; 22:651-671.

Montgomery ML, Case RS. Magnetic resonance imaging of the vascular system: a practical approach for the radiologist. Top Magn Reson Imaging 2003; 14:376-385.

Paschal CB, Morris HD. K-space in the clinic. J Magn Reson Imaging 2004; 19:145-159.

Rohrer M, Geerts-Ossevoort L, Laub G. Technical requirements, biophysical considerations and protocol optimization with magnetic resonance angiography using blood-pool agents. Eur Radiol 2007; 17(Suppl 2):B7-B12.

Shetty AN, Bis KG, Shirkhoda A. Body vascular MR angiography: using two-dimensional and three-dimensional time-of-flight techniques. Concepts Magn Reson 2000; 12:230-255.

Willinek WA, Schild HH. Clinical advantages of 3.0 T MRI over 1.5 T. Eur J Radiol 2008; 65:2-14.

Wilson GJ, Hoogeveen RM, Willinek WA, et al. Parallel imaging in MR angiography. Top Magn Reson Imaging 2004; 15:169-185.

Wright GW. Magnetic resonance imaging. IEEE Signal Process 1997; 14:56-66.

Zhang H, Maki JH, Prince MR. three-dimensional contrast-enhanced MR angiography. J Magn Reson Imaging 2007; 25:13-25.

REFERENCES

1. WR Nitz, MR imaging: acronyms and clinical applications. Eur Radiol 1999; 9:979-997.
2. Miyazaki M, Lee VS. Nonenhanced MR angiography. Radiology 2008; 248:20-43.
3. Macovski A. Noise in MRI . Magn Reson Med 1996; 36:494-497.
4. Gibbs GF, Huston J 3rd, Bernstein MA, et al. Improved image quality of intracranial aneurysms: 3.0-T versus 1.5-T time-of-flight MR angiography. Am J Neuroradiol 2004; 25:84-87.
5. von Morze C, Xu D, Purcell DD, et al. Intracranial time-of-flight MR angiography at 7T with comparison to 3T. J Magn Reson Imaging 2007; 26:900-904.

6. Sodickson DK, Manning WJ. Simultaneous acquisition of spatial harmonics (SMASH): fast imaging with radiofrequency coil arrays. Magn Reson Med 1997; 38:591-603.
7. K. P. Pruessmann, M. Weiger, M. B. Scheidegger, and P. Boesiger, SENSE: sensitivity encoding for fast MRI. Magn Reson Med 1999; 42:952-962.
8. Griswold MA, Jakob PM, Heidemann RM, et al. Generalized autocalibrating partially parallel acquisitions (GRAPPA). Magn Reson Med 2002; 47:1202-1210.
9. Schmitt M, Potthast A, Sosnovik DE, et al. A 128-channel receive-only cardiac coil for highly accelerated cardiac MRI at 3 Tesla. Magn Reson Med 2008; 59:1431-1439.
10. Prince MR, Yucel EK, Kaufman JA, et al. Dynamic gadolinium-enhanced three-dimensional abdominal MR arteriography.J Magn Reson Imaging 1993; 3:877-881.
11. Thomsen HS, Morcos SK, Dawson P. Is there a causal relation between the administration of gadolinium based contrast media and the development of nephrogenic systemic fibrosis (NSF)? Clin Radiol 2006; 61:905-906.
12. Earls JP, Rofsky NM, DeCorato DR, et al. Breath-hold single-dose gadolinium-enhanced three-dimensional MR aortography: usefulness of a timing examination and MR power injector. Radiology 1996; 201:705-710.
13. Foo TKF, Saranathan M, Prince MR, Chenevert TL. Automated detection of bolus arrival and initiation of data acquisition in fast, three-dimensional, gadolinium-enhanced MR angiography. Radiology 1997; 203:275-280.
14. A. H. Wilman, S. J. Riederer, J. Huston, et al. Arterial phase carotid and vertebral artery imaging in three-dimensional contrast-enhanced MR angiography by combining fluoroscopic triggering with an elliptical centric acquisition order. Magn Reson Med 1998; 40:24-35.
15. McGibney G, Smith MR, Nichols ST, Crawley A. Quantitative evaluation of several partial Fourier reconstruction algorithms used in MRI . Magn Reson Med 1993; 30:51-59.
16. Maki JH, Prince MR, Londy FJ, Chenevert TL. The effects of time varying intravascular signal intensity and K-space acquisition order on three-dimensional MR angiography image quality. J Magn Reson Imaging 1996; 6:642-651.
17. Wilman AH. Riederer SJ. Performance of an elliptical centric view order for signal enhancement and motion artifact suppression in breath-hold three-dimensional gradient echo imaging. Magn Reson Med 1997; 38:793-802.
18. Jones RA, Haraldseth O, Muller TB, et al. K-space substitution: a novel dynamic imaging technique, Magn Reson Med 1993; 29:830-834.
19. van Vaals JJ, Brummer ME, Dixon WT, et al. Keyhole method for accelerating imaging of contrast agent uptake. J Magn Reson Imaging 1993; 3:671-675.
20. Bishop JE, Santyr GE, Kelcz F, Plewes DB Limitations of the keyhole technique for quantitative dynamic contrast-enhanced breast MRI . J Magn Reson Imaging 1997; 7:716-723.
21. Korosec FR, Frayne R, Grist TM, Mistretta CA Time-resolved contrast-enhanced three-dimensional MR angiography. Magn Reson Med 1996; 36:345-351.
22. Wehrli FW, Shimakawa A, Gullberg GT, MacFall JR. Time-of-flight MR flow imaging: selective saturation recovery with gradient refocusing. Radiology 1986; 160:781-785.
23. Felmlee JP, Ehman RL. Spatial presaturation: a method for suppressing flow artifacts and improving depiction of vascular anatomy in MR imaging. Radiology 1987; 164:559-564.
24. Dumoulin CL, Souza SP, Walker MF, Wagle W. Three-dimensional phase contrast angiography. Magn Reson Med 1989; 9:139-149.
25. Parker DL, Yuan C, Blatter DD. MR angiography by multiple thin slab three-dimensional acquisition. Magn Reson Med 1991; 17:434-451.
26. Hood MN, Ho VB, Corse WR. Three-dimensional phase-contrast magnetic resonance angiography: A useful clinical adjunct to gadolinium-enhanced three-dimensional renal magnetic resonance angiography? Milit Med 2002; 167:343-349.
27. Moran PR.A flow velocity zeugmatographic interlace for NMRI in humans. Magn Reson Imaging 1982; 1:197-203.
28. Nayler GL, Firmin DN, Longmore DB. Blood flow imaging by cine magnetic resonance. J Comput Assist Tomogr 1986; 10:715-722.
29. Wigstrom L, Sjoqvist L, Wranne B. Temporally resolved three-dimensional phase-contrast imaging. Magn Reson Med 1996; 36:800-803.
30. Haacke EM, Lenz GW. Improving MR image quality in the presence of motion by using rephasing gradients. AJR Am J Roentgenol 1987; 148:1251-1258.
31. Carr JC, Simonetti O, Bundy J, et al. Cine MR angiography of the heart with segmented true fast imaging with steady-state precession. Radiology 2001; 219:828-834.
32. Foo TK, Ho VB, Marcos HB, et al. MR angiography using steady-state free precession. Magn Reson Med 2002; 48:699-706.
33. Jara H, Barish MA. Black-blood MR angiography. Techniques, clinical applications. Magn Reson Imaging Clin North Am 1999; 7:303-317.

AUTHOR QUERY FORM

Dear Author

During the preparation of your manuscript for publication, the questions listed below have arisen. Please attend to these matters and return this form with your proof.

Many thanks for your assistance.

Query References	Query	Remarks
1.	AU: always spelled out in text in this series, per Elsevier style; 3D and 2D not used (but kept in figures).	
2.	AU: Italics used sparingly: e.g., for genus & species, after the word “term” per style.	
3.	AU: OK as edited?	
4.	Au Query: 2D or 3D TOF?	
5.	AU: OK as edited?	
6.	AU: Pls. check cross reference	
7.	AU: Pls. check dosage & initial it	
8.	AU: Pls. check dosage & initial it	
9.	AU: Pls. supply chap. nos.	
10.	AU: Pls. check dosage & initial it	
11.	AU: OK as edited?	
12.	AU: OK as edited?	
13.	AU: OK as edited?	
14.	AU: OK as edited?	
15.	AU: OK as added?	
16.	AU: OK as edited?	
17.	AU: OK as edited, as in figure?	
18.	AU: OK as edited?	
19.	AU: add symbol for this—arrowhead?	
20.	AU: delete labels a and b to be consistent with next figure?	
21.	AU: Please explain A and B.	
22.	AU: asterisks not shown.	
23.	AU: OK as added?	